Design of a Novel Microreactor to Study Short Residence Time Combustion

by

Tianzhu Fan

B.Sc., Dalian University of Technology (P.R. China), 2011

A thesis submitted to the
Faculty of the Graduate School of the
University of Colorado in partial fulfillment
of the requirement for the degree of
Master of Science
Department of Mechanical Engineering
2017

This thesis entitled:
Design of a Novel Microreactor to Study Short Residence Time Combustion
has been approved for the Department of Mechanical Engineering

_____

Dr. Nicole J. Labbe

_____

Dr. John W. Daily

_____

Dr. G. Barney Ellison

Date_____

The final copy of this thesis has been examined by the signatories, and we find that both the content and the form meet acceptable presentation standards of scholarly work in the above-mentioned discipline

Abstract

Tianzhu Fan (M.Sc., Dpt. of Mechanical Engineering)

Design of a Novel Microreactor to Study Short Residence Time Combustion

Thesis directed by Assistant Professor Nicole Labbe

Microreactors are useful tools for understanding the short residence time reactions of biomass polymers and fuel molecules. When coupled with sensitive detection methods, microreactors have the ability to detect all molecules produced in the reactor, including stable, meta-stable, and radical species, making microreactors one of the few experiments where nearly all chemical species may be detected. At the University of Colorado Boulder, our microreactor studies have involved very small (~1 mm internal diameter, ~28 mm long) silicon carbide (SiC) tubes to study short residence time pyrolysis reactions in conjunction with photoionization mass spectrometry (PIMS) and Fourier transform infrared spectroscopy (FTIR). While much has been learned from this configuration, qualitative analysis is hampered by the fact that the pressure and velocity vary greatly within the reactor. To improve the performance of the Boulder microreactor system, this work explores modifying the reactor geometry to achieve better control over the thermofluid properties. Computational fluid dynamics (CFD) simulations were employed to explore how thermofluid properties within the reactor change as a function of reactor geometry, and a converging-nozzle structure was found to be the ideal geometry to control the internal thermodynamic conditions. New reactor prototypes were fabricated based on the simulation results. To verify the results of the CFD simulations for the new reactor geometry, a series of experiments are proposed to compare

the performance of the original Boulder reactors with the new prototype reactors. These experiments will be conducted with the reactors installed in the PIMS configuration. Finally, a survey of potential alternative micro-reactor materials was conducted for future microreactor development. Currently, the SiC microreactor is limited to thermal decomposition experiments due to SiC reactivity with oxygen. To move towards oxidation experiments, a new material for the microreactor must be identified. Thermal conductivity, structural stability, and non-reactivity were all considered in the survey. The new microreactor designed in this thesis will assist scholars to carry out fundamental kinetic measurements of short residence time oxidation reactions of fuels in the future, which will lead a deeper understanding of fuel properties and promote the development of new fuel efficient, less-polluting engine technology.

DEDICATIONS

This thesis is dedicated,

to all persons who helped me finish the research - my thesis advisor Dr. Nicole Labbe for her diligent and professional guidance, my thesis committee members Dr. John W. Daily & Dr. G. Barney Ellison for their suggestions and advice during my research progress, and my friends Ms. Katherine Cummins & Mr. Cory Rogers for their help with running experiments and thesis writing.

to my parents, whose love and unselfish support over twenty years made me strong and proud, and my love, Ziyang, who brings sunlight to my life.

to Skyamuni Buddha, who tells me the truth of this world:

"A real mind come out when you ignore anything visible"

——《The Vajracchedika-prajna-paramita Sutra》

致谢 (DEDICATIONS)

我谨将此论文，

献于所有帮助我完成此研究的人 – 包括给予我勤勉指导的导师 Dr. Nicole Labbe, 在研究过程中提出宝贵意见的教授 Dr. John W. Daily 和 Dr. G. Barney Ellison，以及协助我完成实验和论文撰写的同研 Ms. Katherine Cummins 和 Mr. Cory Rogers.

献于二十多年来一直给予我无私支持的父母，是他们的爱让我变得强壮和自豪。献于我的挚爱 – 为我生命带来一缕阳光的子扬。

献于启迪我的释迦摩尼佛:

“应无所住而生其心”

——《金刚般若波罗蜜经》

ACKNOWLEDGEMENT

This research was funded through CU Boulder via the startup funds of Dr. Nicole Labbe. Support for John W. Daily and G. Barney Ellison as well as Cory O. Rogers was provided through NSF Grant CBET-1403979.

CONTENTS

CHAPTER

TABLES

Table

FIGURES

Figure

CHAPTER 1

INTRODUCTION

1.1 Purpose of the Study

Combustion is an essential process for energy generation today. Nowadays, traditional thermal power still occupies around 64% power output of the market share in the United States (in 2016, the total electric generation in U.S was around $4.08\times10^6 MW$, where $2.62\times10^6 MW$ came from consuming coal, natural gas, and other fossil fuels)[1]. Also, vehicles with internal combustion engines (ICE) will be the dominant mode of transportation in the foreseeable future. However, energy resources such as traditional petroleum fuels, currently face the serious problems including resource depletion, greenhouse gas production, and harmful emissions such as SO_x and NO_x. As a result, some countries now suffer from considerable pollution problems stemming from respirable air particles (PM2.5 and PM5.0)[2], which damage people's health and harm society's confidence in combustion of traditional fuels. Thus, developing alternative clean renewable fuels to replace traditional fuels is a critical mission for human-beings.

[1] "Electric Power Monthly with Data for July 2017." *U.S. Energy Information Administration*

[2] Brown, James S., et al. "Thoracic and respirable particle definitions for human health risk assessment." *Particle and fibre toxicology* 10.1 (2013): 12.

Biofuels are a potential solution to provide a renewable alternative liquid fuel source for traditional combustion engine technology. Without sulfur and nitrogen elements, biofuels can be renewably refined from living organisms and tend to produce fewer harmful emissions, which helps address the limited resource and pollution problems. Some reliable and developed biofuels, such as biodiesel and ethanol, are already widely applied today. In the U.S., some novel thermal power plants are now combusting biomethane, which is produced through fermentation of organic waste by microorganisms, to generate electric power. Additionally, almost all gas stations provide gasoline as a blend including 10% ethanol.

Biofuels provide hope as a renewable liquid fuel source, yet there several challenges to their adoption as a full petroleum fuel replacement. In particular, biofuels usually have lower energy density (due to their lower carbon proportions) and suffer inefficient industrial production. Also, people are still uncertain about the propensity for biofuels to form pollutants, especially for incomplete combustion cases. Therefore, understanding the fundamental chemistry pathways for combustion for both biofuels and traditional petrochemical fuels is one of the significant methods leading to the engineering of alternative renewable fuels that overcome these challenges.

Pyrolytic microreactors coupled with sensitive chemical detection methods, such as the one developed by G. Barney Ellison at the University of Colorado Boulder, have the ability to probe the fundamental chemistry of most fuels, including both traditional and renewable fuels. The experiments conducted with the Ellison microreactor typically detect the products of chemical reactions after very short residence times (~100μs). Powerful diagnostic capabilities such as photoionzation mass spectrometry (PIMS) and Fourier transform infrared spectroscopy (IR) are used to analyze the products from the reactor, including the radical and meta-stable products. The Ellison microreactor, which is based on a Chen-Nozzle[3], is shown in Figure 1. These microreactors typically have a very small diameter (~ 1mm) and a length of 2-3 cm, which is comparable to the diameter of a quarter. This system has been used to study the pyrolysis chemistry of several biofuels to date in the past three years, including benzyl radical[4] ($C_6H_5CH_2$), cycloheptatrienyl radical [5] (C_7H_7), 2-methoxyfuran [6] (2-MeOF)

[3] Chen, Peter, et al. "Flash pyrolytic production of rotationally cold free radicals in a supersonic jet. Resonant multiphoton spectrum of the 3p2A2". rarw. X2A2" origin band of methyl." *The Journal of Physical Chemistry* 90.11 (1986): 2319-2321.

[4] Buckingham, Grant T., et al. "The thermal decomposition of the benzyl radical in a heated micro-reactor. I. Experimental findings." *The Journal of chemical physics* 142.4 (2015): 044307.

[5] Buckingham, Grant T., et al. "The thermal decomposition of the benzyl radical in a heated micro-reactor. II. Pyrolysis of the tropyl radical." *The Journal of chemical physics* 145.1 (2016): 014305.

[6] Urness, Kimberly N., et al. "Pyrolysis Pathways of the Furanic Ether 2-Methoxyfuran." *The Journal of Physical Chemistry A*119.39 (2015): 9962-9977.

cyclohexanone [7] (C_6H_{10}=O), glycolaldehyde [8] (CHO-CH_2OH) and methyl acetate[9] (CH_3COOCH_3)

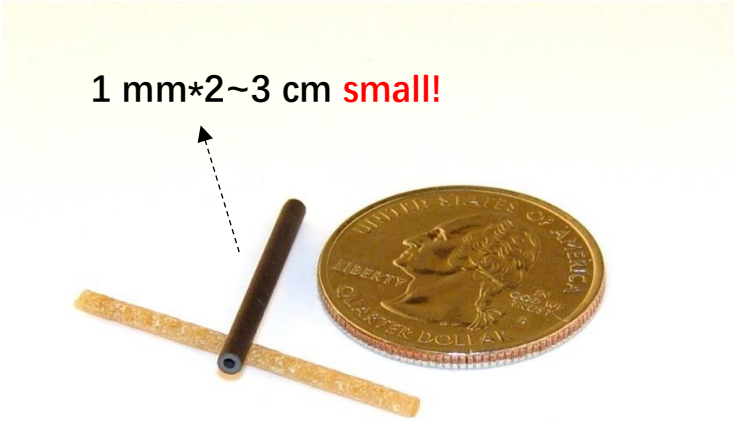

Figure 1: Microreactor currently used at the University of Colorado

1.2 Scope of the Study

While the Ellison microreactor has been successful in elucidating the chemistry of several fuels to date, the focus of this work is to improve the existing capabilities of the Ellison microreactor experiment by reducing systematic uncertainties and provide the ability to conduct oxidation

[7] Porterfield, Jessica P., et al. "Isomerization and fragmentation of cyclohexanone in a heated micro-reactor." *The Journal of Physical Chemistry A* 119.51 (2015): 12635-12647.

[8] Porterfield, Jessica P., et al. "Pyrolysis of the Simplest Carbohydrate, Glycolaldehyde (CHO− CH2OH), and Glyoxal in a Heated Microreactor." *The Journal of Physical Chemistry A* 120.14 (2016): 2161-2172.

[9] Porterfield, Jessica P., et al. "Thermal Decomposition of Potential Ester Biofuels Part I: Methyl Acetate and Methyl Butanoate." *The Journal of Physical Chemistry A* (2017).

experiments through a microreactor structure redesign. This work was conducted in three parts: 1) computational fluid dynamics was leveraged to redesign the microreactor structure using thermodynamics design principles to stabilize the thermodynamic conditions within the microreactor, 2) new materials were identified to fabricate the new microreactor to maintain structural integrity at high temperature while being non-reactive, and 3) a prototype of the new microreactor was fabricated and installed in the existing PIMS experimental setup for initial testing and direct comparison to the original microreactor.

This work may be organized into two distinct thrusts, the first of which consists of the computational design efforts. The design thrust includes structural design and materials selection respectively. The microreactor structure was redesigned using Computational Fluid Dynamics (CFD) method to predict the reactor thermodynamic performance and identify an ideal microreactor geometry that yields steady temperature, pressure, and velocity profiles along the length of the reactor. The material design focused on a materials properties investigation and selection, considering factors such as structural stability, thermal conductivity, and reactivity under high temperature conditions. The second thrust focuses on the experimental testing of a prototype microreactor designed based on the results of the design thrust. A microreactor was fabricated based on the results of the

CFD work and installed into the existing PIMS experimental setup. A series of fuels were tested using both the original Ellison microreactor and the new microreactor to directly compare the performance of both reactors. As a direct result of this research, this redesigned microreactor system will be leveraged to conduct first-of-its-kind fundamental research on the short residence time oxidation reactions of fuels.

CHAPTER 2

BACKGROUND

2.1 The "Chen-Nozzle"

A microreactor is generally described as a single tube or a series of interconnecting channels in a planar surface in which chemical reactions take place. Microreactors carry out chemical reactions in a confinement for a specified period of time by controlled reactants mixing sequences. The products can be analyzed by various diagnostic technologies such as gas chromatographic-flame ionization detection (GC-FID), photoionization mass spectrometry (PIMS), or Fourier transform infrared spectroscopy (FTIR) [10] . Statistics show more than half of reactions in the fine chemical/pharmaceutical industry are performed using a microreactor system[11].

There are advantages to using a microreactor to study chemical composition. The small inner diameter of the microreactor allows for laminar fluid flow, a high liquid-solid heat transfer coefficient, and relatively large reactants surface-to-volume ratio when compared to conventional scale reactors. This

[10] Haswell, Stephen J., et al. "The application of micro reactors to synthetic chemistry." *Chemical Communications* 5 (2001): 391-398.

[11] Roberge, Dominique M., et al. "Microreactor technology: a revolution for the fine chemical and pharmaceutical industries?" *Chemical engineering & technology* 28.3 (2005): 318-323.

allows reactions to happen several times faster than those in larger scale reactors. Researchers can achieve local concentration control, product separation, and side-reaction prevention by adjusting reactant injection volume, thermodynamic environment, and residence time of the reactions. Also, since hazardous products recovery and treatment is an intractable problem for traditional chemistry experiments, microreactor systems may be beneficial since they generate very few products, implement the reactions in a completely enclosed space, and exhaust all chemicals in gaseous form to be treated as necessary.

A microreactor named the "Chen nozzle"[12] was first proposed and applied for testing by Peter Chen in 1978. The original "Chen nozzle" is a supersonic jet made by alumina (Al_2O_3) with a length of 30 mm and a 1.0 mm internal diameter. It was first used to carry out flash pyrolysis of tert-butyl nitrite. The main products, methyl radicals, were ionized by vacuum-UV light at 10.5 eV and detected by mass-time-of-flight spectrometry. In 1992, Chen's group used his nozzle design to perform additional flash pyrolysis experiments studying radicals, carbenes, and biradicals. Now, the "Chen nozzle" has become a recognized tool to study pyrolysis of organic

[12] Chen, Peter, et al. "Flash pyrolytic production of rotationally cold free radicals in a supersonic jet. Resonant multiphoton spectrum of the 3p2A2". rarw. X2A2" origin band of methyl." *The Journal of Physical Chemistry* 90.11 (1986): 2319-2321.

molecules[13].

Over the past few decades at the University of Colorado Boulder, Prof. John W. Daily and Prof. G. Barney Elision have worked to develop an improved "Chen nozzle" constructed of silicon carbon for better performance at high temperatures. This improved nozzle has been coupled with PIMS and FTIR diagnosis systems and has become a powerful instrument to analyze the pyrolysis processes of many complex organic biofuels. The complete system with the improved nozzle will be presented in following sections in greater detail.

2.2 Photoionization Mass Spectrometry (PIMS)

2.2.1 Single Photon Ionization Technology

Single photon ionization (SPI) with coherent vacuum ultraviolet (VUV) is a powerful tool used in a number of chemical analysis experiments. Compared with multi photon ionization (MPI) technology, SPI has less possibility to induce fragmentation, which is due to the combination of additional photons by ions, which can cloud the analytical results[14]. Therefore, SPI technology coupled with a time-of-flight mass spectra (TFS) system has been widely

[13] Blush, Joel A., et al. "Photoionization mass and photoelectron spectroscopy of radicals, carbenes, and biradicals." *Accounts of chemical research* 25.9 (1992): 385-392.

[14] Lockyer, Nicholas P., and John C. Vickerman. "Single photon ionisation mass spectrometry using laser-generated vacuum ultraviolet photons." *Laser Chemistry* 17.3 (1997): 139-159.

applied to analyze the components of chemicals, drugs, and biological cells in the United States[15].

The principle of SPI – third harmonic conversion is explained in the following. In a monatomic gas environment, a third harmonic ion beam will be generated when an incident photon is absorbed by a molecule in the nonlinear medium. The power of the third harmonic radiation is given by,

$$P_{3w} = N^2 \cdot \left|{x_a}^{(3)}\right|^2 \cdot {P_w}^2 \cdot F(L, b, \Delta k) \quad (1)$$

$$\mathrm{b} = \frac{2\pi {w_o}^2}{\lambda} \quad (2)$$

where N is the number density, ${x_a}^{(3)}$ is the third order nonlinear susceptibility, P_w is the incident photon power, and $F(L, b, \Delta k)$ is the geometrical factor. The third harmonic ion beam will only be generated in a specific wavelength range for each given gas, but almost all organic molecules can be ionized by an energy level of 10.5 eV, which corresponds to a 118.2 nm wavelength. Therefore, a frequency tripling process is needed since commercial laser sources typically cannot provide photons at this wavelength[16]. A photon ionization system with tripling cell is shown in

[15] Van Bramer, S. E., and M. V. Johnston. "Tunable, coherent vacuum ultraviolet radiation for photoionization mass spectrometry." *Applied spectroscopy* 46.2 (1992): 255-261.

[16] Steenvoorden, R. J. J. M., et al. "Laser single photon ionization mass spectrometry of linear, branched and cyclic hexanes." *International Journal of Mass Spectrometry and Ion Processes*107.3 (1991): 475-489.

Figure 2. The 355-nm correctional laser from Nd: YAG laser, passes through the silicon carbon mirrors, is tripled to 118.2 nm in the atmosphere of Ar and Xe, and then is focused to the detection cell zone by the magnesium fluoride mirror.

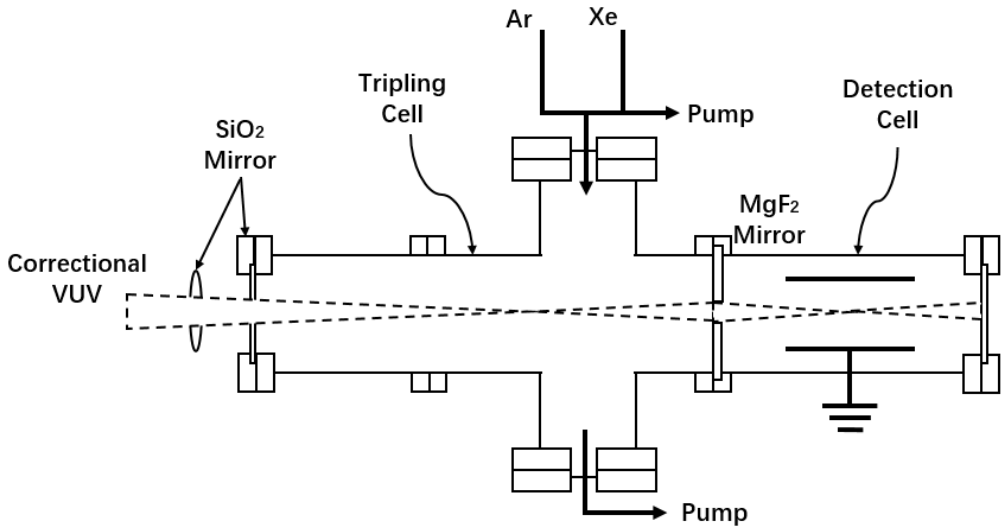

Figure 2: Photon ionization system with tripling cell

The geometrical factor, F, must be adjusted to maximize ion beam power during the testing, which ensures the TOF system can receive the signal. Several other systems must be optimized as well, including the pressure and concentration of the Ar/Xe atmosphere, the focus length of the magnesium fluoride (MgF_2) mirror, and the voltage and direction of the picoammeter in the detection cell.

2.2.2 Time-of-Flight Mass Spectrometry Technology

Molecules ionized by photons in the detection zone are then analyzed by a time-of-flight mass spectrometer (ToF-MS). In recent years, researchers have benefited from ToF-MS technology due to its rapid, high resolution molecular mass analysis functionality with unlimited mass range[17]. A ToF-MS instrument has three distinct regions, a source-extraction region, a drift region, and a detection region, which are shown in Figure 3. The ions generated in the source region are imposed by a forward voltage causing an increase in kinetic energy described following equation.[18]

$$\frac{mv^2}{2} = eV \tag{3}$$

Where m is the ion's mass, v is the ion's velocity, V is the forward voltage, and e represents the elementary charge constant, which is approximately equal to $1.602\times10^{-19}\,coulombs$. Ions with an initial velocity then fly through the drift region and are eventually caught by the detector. The flight time for ions is recorded by a digital oscilloscope and can be calculated using,

[17] Mamyrin, B. A., et al. "The massreflect ron, a new non-magnetic time-of-flight mass spectrometer with high resolution." *Zh. Eksp. Teor. Fiz* 64 (1973): 82-89.

[18] Mamyrin, B. A. "Time-of-flight mass spectrometry (concepts, achievements, and prospects)." *International Journal of Mass Spectrometry* 206.3 (2001): 251-266.

$$t = \left(\frac{m}{2eV}\right)^{1/2} \cdot D \quad (4)$$

where D is the length of the drift region. Therefore, the mass of specific molecules can be calculated according to their flight time, length of drift region, and forward voltage.

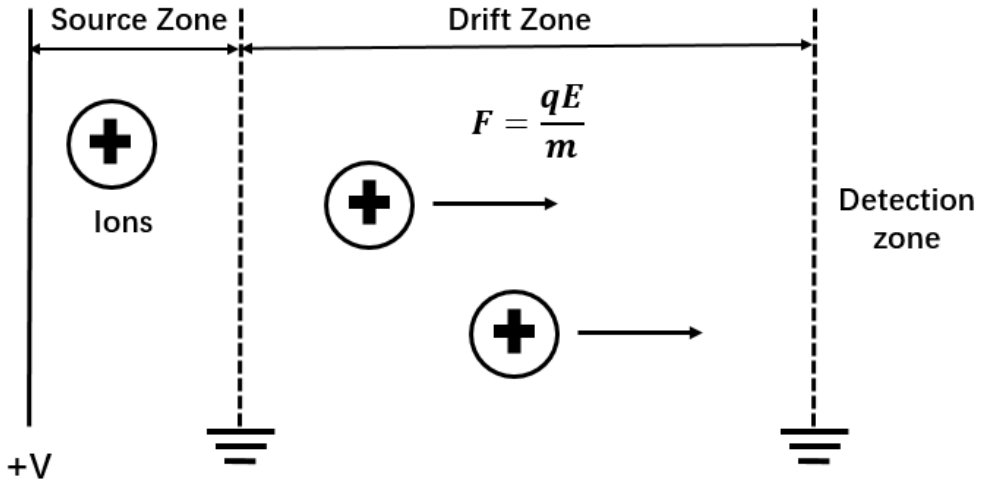

Figure 3: Diagram for time-of-flight mass spectrometer

Initial ToF-MS instruments did not attract many researchers because the technology suffered from low resolution and accuracy due to the uncertainty of flight time, space, and kinetic energy distributions. Fortunately, these problems have been resolve by recent ToF-MS technological innovation. For time distributions, two ions which have been generated in different times in the source-extraction region will result in another temporal difference, Δt, for detector absorption, which can be addressed by enhancing the length

of the drift region, D, to minimize the effect of temporal differences. Ions have an initial kinetic energy, KE_{ini}, when ionized, so, the actual kinetic energy of the ions when reaching the detector is $\mathrm{KE} = \mathrm{eV} + KE_{ini}$ instead of just $1\ \mathrm{eV}$. To eliminate the influence of initial kinetic energy, the accelerating voltage is improved to ensure that $1\ \mathrm{eV}$ is much greater than KE_{ini}.

2.3 Fourier Transform Infrared Spectroscopy (FTIR)

As a general principle of modern physics, molecules have different ionization energies based on their total number of electrons, vibrations, and rotations, and each molecule will be excited to a higher energy level when absorbing energy from a single photon given by,

$$\mathrm{h}\nu = E_n - E_m \tag{5}$$

where E_n denotes the higher energy level and E_m denotes the lower energy level. To be excited, molecules can only absorb single photons with a series of specific energy levels, $\mathrm{h}\nu$, which are exactly equal to the energy gaps. Therefore, molecules can be identified by determining the frequency and wavelength of the lights they are able to absorb. This can also be extended to functional groups structure identification of complex organic molecules. Infrared Spectrometry (IR) is a common tool used to analyze

organic molecule structures and chemical properties using the theory described above[19]. As a kind of nondispersive IR instrument, a Fourier Transform Infrared Spectrometry (FTIR) system applies an interferometer to encode data from the whole spectral range simultaneously. A general FTIR system typically includes an infrared light source, a Michelson interferometer, a sample compartment, and a detection system. A schematic representation of FTIR system is shown in Figure 4.

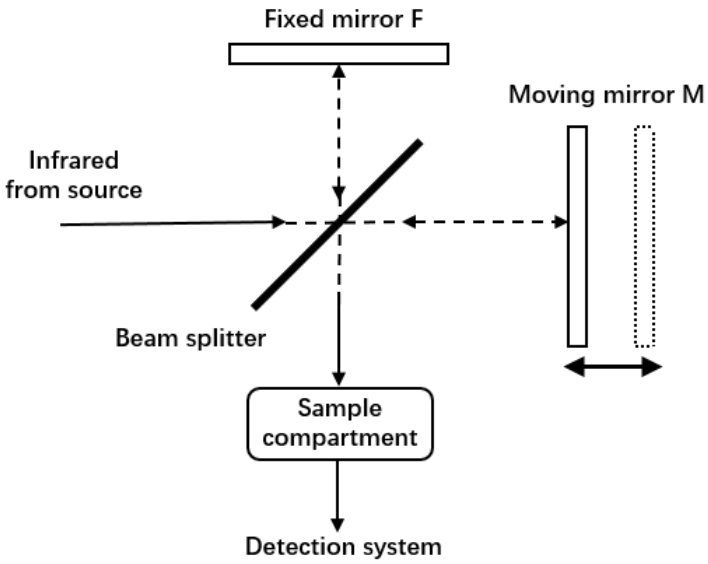

Figure 4: A schematic representation of an FTIR system

Radiation from the source goes through a beam splitter and is separated into two beams with 50 percent dedicated to transmission and the other 50

[19] Susi, Heino, and D. Michael Byler. "[13] Resolution-enhanced fourier transform infrared spectroscopy of enzymes." *Methods in enzymology* 130 (1986): 290-311.

percent to reflection. The two beams are then reflected and recombine at the beam splitter. The intensity of the recombined beam is determined by the wavelength and the retardation of the beams, which is the difference of their path lengths. The intensity of a monochromatic beam can be described as follows,

$$\mathrm{I}(\delta) = B(\nu)\cos(2\pi\check{\nu}\delta) \tag{6}$$

where $\check{\nu}$ denotes the wavenumber, δ denotes the retardation, and $B(\nu)$ denotes the intensity as a function of light frequency. Therefore, the desired intensity signal could be achieved by adjusting the retardation, that is, the position of the moving mirror for a specific infrared beam. A specific frequency decrease will be shown in the interferogram, which is then transformed from a "time domain" to a "frequency domain" using a Fourier Transform if it has been absorbed by a specific functional group of organic samples. The following equation is the Fourier transform indicating time-frequency conversion.

$$\mathrm{F}(\nu) = \frac{1}{\sqrt{2\pi}}\int_{-\infty}^{\infty} f(t)\cos(2\pi\nu t)\,dt \tag{7}$$

Hence, frequency spectrums generated by the detection system (including an amplifier, a DC/AC converter and a computer) can analyze the structures

and compounds found in a sample. Modern FTIR instruments have *Jacquinot's advantage*, *Fellgett's advantage* and *Conne's advantage*[20], which relatively correspond to abilities and superiorities of higher throughput than dispersive instruments, providing a whole spectrum immediately, and indexing retardation by a monochromatic beam precisely. FTIR instruments still have a reputation for fussy spectrum analysis and limited quantification analysis, which means sometimes researchers cannot clarify a sample's makeup with a single IR spectrum and cannot achieve qualitative analysis under extreme conditions such as very low or high concentrations.

2.4 History of the PIMS and IR Microreactor Systems at the University of Colorado and other Institutes.

In 2003, Xu Zhang, G. Barney Ellison et al.[21] successfully used a pulsed supersonic nozzle to study the thermal decomposition of allyl radicals (CH_2CHCH_2) and methyl-peroxyl radicals (CH_2OO) with matrix-isolated infrared spectroscopy. A major difficulty with matrix IR is the capability to obtain clean and accurate spectra since sometimes the desired radicals are obscured by by-products, secondary reaction products, or unwanted

[20] Christy, Alfred A., Yukihiro Ozaki, and Vasilis G. Gregoriou. *Modern Fourier transform infrared spectroscopy*. Elsevier, 2001.

[21] Zhang, Xu, et al. "Intense, hyperthermal source of organic radicals for matrix-isolation spectroscopy." *Review of scientific instruments* 74.6 (2003): 3077-3086.

photoproducts (which can be avoided by pulsing a supersonic nozzle with intense light sources, allowing for very short contact time (30 μs) to avoid secondary radical-radical reactions and other unpredictable reactions). As a result, allyl radical (CH_2CHCH_2) were observed in matrix IR spectra by exploring several precursors, which include CH_2=$CHCH_2I$ and CH_2=$CHCH_2CH_2CH$=CH_2, at around 1150 K. Methyl-peroxyl radicals (CH_2OO) were obtained using azomethane (CH_3NNCH_3) as a precursor.

In 2009, to research the role furans played in polycyclic aromatic hydrocarbon (PAH) formation in biomass gasification, Vasiliou, Ellison, et al.[22] implemented a study of furan thermal decomposition under various temperature and pressure conditions using a tubular silicon carbide reactor with both PIMS and FTIR diagnostics. Some initial products were observed, which were predicted by pervious G2(MP2) electronic structure theory calculations. (CO + CH_3CCH) and (HCCH + CH_2CO) are the first dissociation products of furan at about 1350 K, and when temperatures were increased to around 1550 K, propargyl radicals (CH_2CCH) were also detected. The experimental results demonstrated that the process of furan decomposition is also dependent on the pressure in the tubular reactors. For instance, at higher pressures, radicals participate in additional reactions

[22] Vasiliou, AnGayle, et al. "Thermal decomposition of furan generates propargyl radicals." *The Journal of Physical Chemistry A* 113.30 (2009): 8540-8547.

that produce aromatic gasification products like benzene and styrene.

In 2012, Vasiliou, Ellison, et al.[23] used a heated microtubular reactor to study the thermal decomposition of CH_3CHO, which was already well-studied by previous researchers, and its isotopomers over very short residence times (100-200 μs) and temperature range of 1200 to 1900 K. Many products were found in the decomposition of acetaldehyde including H_2, CH_3, CO, and H_2O. It is believed that auxiliary bimolecular reactions generate other byproducts such as HC=CH and CH_2=C=O. The reactions of CH_3CDO, CD_3CHO and CD_3CDO were also analyzed and proved that their dissociation is comparable to CH_3CHO. This research provided a correction of the existing Rice-Herzfeld scheme[24] and furthermore developed a more detailed explanation for decomposition process of acetaldehyde.

In 2013, to study the properties of 2-methylfuran (2MF) and 2,5-dimethylfuran, which have been considered as alternatives fuels to substitute gasoline in internal combustion engine (ICE), Urness, Ellison, et al.[25] used a PIMS system to research the decomposition reactions of furan,

---

[23] Vasiliou, AnGayle K., et al. "Thermal decomposition of CH3CHO studied by matrix infrared spectroscopy and photoionization mass spectroscopy." *The Journal of chemical physics* 137.16 (2012): 164308.

[24] Laidler, K. J., and M. T. H. Liu. "The mechanism of the acetaldehyde pyrolysis." *Proceedings of the Royal Society of London A: Mathematical, Physical and Engineering Sciences*. Vol. 297. No. 1450. The Royal Society, 1967.

[25] Urness, Kimberly N., et al. "Pyrolysis of furan in a microreactor." *The Journal of*

which has a similar structure and properties to 2MF and DMF. Two pyrolysis products of furan, α-carbene and β-carbene, were discovered. To distinguish the ratio between the two main products, researchers applied the potential of the PIMS system to evaluate the number density of molecules of both products using the following equation,

$$n_i = \frac{{S_i}^+}{CD_i\varphi(E)\sigma_i(E)} \quad (8)$$

where ${S_i}^+$ is the signal intensity, C is the constant representing all the geometry dependent factors, D_i is the mass discrimination factor, $\varphi(E)$ is the photon flux, and $\sigma_i(E)$ is the energy-dependent molecular photoionization cross section. By applying the above equation, researchers compared the ratio between α-carbene and β-carbene, and reported around 80% of furan decomposes to β-carbene independent of temperature.

Using the same methods, in 2015, scholars[26] researched the unimolecular decomposition mechanism of 2-methoxyfuran, which is a secondary biofuel derived from nonedible biomass. The primary products observed included H, CH_3, CO, HC=CH, and 2-furanyloxy radicals. The secondary biomolecular reactions between 2-methoxyfuran/2-furanyloxy and H/CH_3

chemical physics 139.12 (2013): 124305.

[26] Urness, Kimberly N., et al. "Pyrolysis Pathways of the Furanic Ether 2-Methoxyfuran." *The Journal of Physical Chemistry A*119.39 (2015): 9962-9977.

radicals were investigated and shown to generate other organic byproducts such as CH_2=CHCHO, CH_3CH=CHCHO, and CH_3COCH=CH_2. Similarly, applying Eq. 8, scholars discovered that only 1-3% of 2-methoxyfuran are involved in the secondary reactions depending on reactants concentration and pressure in the reactor.

In Ref. [9] of 2017, to determine the thermal cracking rules of fatty acid methyl esters, which have similar combustion properties of traditional fuels, Porterfield, Ellison, et al. used SiC microreactors to study unimolecular reactions of two representative prototypes, methyl acetate and methyl butanoate, from 300 to 1600 K at 20 Torr. The study showed that methyl acetate decomposes to methanol and ketene at 1000 K. When it was heated to 1300 K, other products including CH_3, CO, CH_2=O and CO_2 were found. For $CH_3CH_2CH_2COOCH_3$, methanol and ethyl ketene were obtained as the pyrolysis products at 800 K, and a more complicated set of radicals appeared at 1300 K. Following the trends observed in this research, Porterfield et al. generalized the fundamental decomposition paths of RCH_2-$COOCH_3$, which is a generalized fatty acid methyl ester. A 4-centered elimination of methanol to form a ketene is the most significant thermal cracking path.

The above materials have presented highlights from the research conducted at the University of Colorado Boulder on the thermal decomposition of

biofuels using a microreactor coupled with PIMS and IR detection methods. Other institutes have conducted similar research. At the National Renewable Energy Laboratory in 2011, Jarvis, Daily, et al.[27] were the first to use a PIMS and matrix-IR system to study pyrolysis reactions of 2-phenethyl phenyl ether (PPE) and phenyl ethyl ether (PEE) in a hyperthermal nozzle. In summary, the C-O bond homolysis was the main pathway to generate phenoxy radical, cyclopentadienyl radical, and benzyl radical as PPE decomposition products, especially under high temperature (> 1000 K), while C-C bond homolysis is inconsequential at all temperatures.

In 2008, at the University of Science and Technology of China, Zhang, Qi, et al.[28] applied molecular-beam mass spectrometry (MBMS) to understand the high temperature chemistry of methyl tert-butyl ether (MTBE) by studying its pyrolysis reactions from 700 to 1400 K. The observed the main products included H_2, CO, CH_4, CH_3OH, and C_4H_8, as well as other radicals. The mole fraction profiles of major species at different temperatures were also measured.

---

[27] Jarvis, Mark W., et al. "Direct detection of products from the pyrolysis of 2-phenethyl phenyl ether." *The Journal of Physical Chemistry A* 115.4 (2011): 428-438.

[28] Zhang, Taichang, et al. "Pyrolysis of methyl tert-butyl ether (MTBE). 1. Experimental study with molecular-beam mass spectrometry and tunable synchrotron VUV photoionization." *The Journal of Physical Chemistry A* 112.42 (2008): 10487-10494.

As discussed above, micro-reactors have been widely used to research the chemistry of organic biofuels. While, the thermodynamic properties in micro-reactors such as temperature, pressure, and velocity distributions, have significant impact on experimental results, they had never been focused on until Guan, Daily, et al.[29] studied the properties of a micro-reactor for unimolecular decomposition of large molecules using computational fluid dynamics (CFD) simulations in 2013. They applied the general Navier-Stokers equation to solve for the thermodynamic property profiles of several typical classical micro-reactors in the PIMS configuration using both He and Ar as carrier gases. Center line profiles and radial profiles were obtained by varying wall temperature and mass flow rate. Having accurate thermodynamic distributions allows for reaction kinetics information to be obtained. Here, cyclohexene decomposition and methoxy furan pyrolysis were selected as the examples to demonstrate how their reaction rates and mole fractions change with reactors.

The above research provided detailed descriptions and explanations of thermodynamic property distributions in classical reactors and their influence on pyrolysis reactions. However, since the classical reactor's structure is tubular-like, the reacting flow travels from a high-pressure

[29] Guan, Qi, et al. "The properties of a micro-reactor for the study of the unimolecular decomposition of large molecules." *International Reviews in Physical Chemistry* 33.4 (2014): 447-487.

upstream region to a downstream vacuum chamber, resulting in a dramatic pressure drop and considerable velocity increase across the length of the reactor. Providing a stabilized pressure environment and controlling reaction residence time are hard to achieve, which are both major deficiencies of the current system. We thereby propose a novel reactor structure and verify its thermal performance in this thesis with the detailed research and techniques described in the following sections.

CHAPTER 3

METHODS

While the current microreactor system has proven to be a useful experiment to study chemical mechanisms for the unimolecular dissociation of many fuels, the system has limitations which warrant a closer look at the design of this apparatus. The current micro-reactor is made of silicon carbon (SiC) which is reactive with oxygen, making the material a major impediment to studying reactive conditions other than pyrolysis. One design change being considered is to build the microreactor out of a non-reactive material to carry out oxidation studies. Thereby, materials with appropriate properties such as stability, thermal conductivity, and durability when exposed to high temperatures are investigated and selected. The process and findings of this detailed investigation can be found in Chapter 4. In this chapter, however, we focus on the details of the numerical methods used to design a new microreactor with controlled thermodynamic properties as well as the experimental procedures for testing the new microreactors fabricated in this work.

3.1 Numerical Methods for Reactor Design

Another issue with the current design of the microreactor that is the pressure and temperature profiles vary drastically along the tube length. Reconfiguring the microreactor geometry to stabilize the pressure and

temperature profiles is desirable to reduce the uncertainty of reaction parameters. Theoretical and numerical models were used to study the effects of reconfigured geometry and predict the reactor thermodynamic performance.

Theoretical models in different fields of fluid dynamics have been well-developed over the past few decades. Researchers are now able to simplify complex cases and problems, particularly for laminar flows, and provide a qualitative prediction for fluid behavior in systems. Here, theoretical models are used to analyze the current system's deficiencies, and from that, identify improvement strategies for the novel microreactor design.

The current microreactor geometry is that of a simple cylindrical tube with a length and internal diameter of 25 mm and 1.0 mm respectively. The flow within the tube is laminar, and thus the pressure drop, ΔP, along the reactor can be represented by the following equations[30],

$$\Delta P = \frac{\overline{f_{fd,h}} \cdot L \cdot \rho \cdot \left|\vec{U}\right|^2}{2D} \tag{9}$$

[30] Holman, Jack P. Heat transfer. Vol. 2. New York: McGraw-hill, 1986.

$$\overline{f_{fd,h}} = \frac{64}{Re_D} \tag{10}$$

where $f_{fd,h}$ is the friction factor, L and D are the length and internal diameter of the cylindrical tube, and Re_D is the Reynold number for internal flow. When we consider typical inlet mass flow rates in the current system, Eqs. 9 & 10 show the pressure continuously drops from an inlet pressure of around 0.1-0.3 atm to a vacuum along the reactor centerline, and thus, the pressure profile spans several orders of magnitude. To achieve a more uniform pressure profile within the microreactor, we propose adding a converging-diverging nozzle structure at the outlet of the reactor's main body (see Fig. 5). Converging or converging-diverging nozzles are often used in other engineering applications (e.g. aircraft propulsion) due to their ability to control flow rates and pressures. An equation relating mass flow rate and the choke diameter for isentropic flow in a converging nozzle is found in Eq. 11[31].

$$\dot{m} = A * P_0 * \sqrt{\frac{\gamma}{RT_0}} \left(\frac{2}{\gamma+1}\right)^{\frac{\gamma+1}{2(\gamma-1)}} \tag{11}$$

[31] Cengel, Yunus A., and Michael A. Boles. "Thermodynamics: an engineering approach." Sea 1000 (2002): 8862.

where $\dot{m}$ is the mass flow rate, A is the nozzle outlet area, P_0 is the upstream pressure, and γ is the ratio of specific heats. Eq. 11 shows that upstream pressure may be controlled by changing the choke area while mass flow rate is held constant. Fig. 5 outlines the important geometric variables we believe will have an effect on the internal flow. These geometric parameters include the length of the cylindrical tube, L, the exit diameter of the converging nozzle, d, and the lengths of both the converging and diverging nozzles, G1 and G2, respectively. In this study, we have held the diameter of the main body constant. Optimizing these variables will help determine the final geometry of the improved micro-reactor.

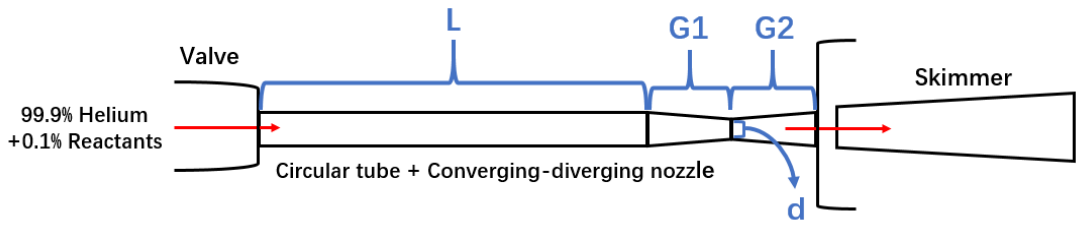

Figure 5: Novel micro-reactor structure design diagram

Due to the complexity of the reactor's internal flow conditions, such as high-velocity, compressible flow, and limited reaction space (small inner diameter), the theoretical model is not accurate enough to provide the resolution needed for the redesign of the microreactor system. To overcome this difficulty, advanced numerical models may be used to obtain higher

fidelity results as necessary for the design applications, while using only modest computational resources. The most popular numerical method to solve fluid mechanics problems is the Computational Fluid Dynamics (CFD) method. The idea was first proposed in 1950 and has been advanced drastically in recent years. Available CFD software includes commercial products and open-source software, allowing researchers to solve fluid problems precisely and rapidly. CFD methods were utilized to design the novel microreactor structure based on the internal flow parameters and properties.

For the computational fluid dynamics calculations, we select helium as the carrier gas because it is non-reactive, monatomic, and has a relatively high thermal conductivity. To date, experiments have been conducted under very dilute conditions (≤ 0.1 mol% reactant in He) to ensure only unimolecular reactions occur, so in our CFD simulations we assume the inlet gas is pure helium. The continuity equation, conservation of linear momentum equation, and conservation of energy equation for steady-state, compressible, ideal gas flow are described as follows[32],

$$\nabla \cdot \left(\rho \vec{U}\right) = 0 \qquad (12)$$

[32] Moukalled, F., L. Mangani, and M. Darwish. "The finite volume method in computational fluid dynamics." (2016).

$$\rho(\vec{U}\cdot\nabla)\vec{U} = \vec{f} - \nabla p + \mu\nabla^2\vec{U} - \frac{2}{3}\mu\nabla(\nabla\cdot\vec{U}) \quad (13)$$

$$c_p\nabla\cdot(\rho\vec{U}T) = \nabla\cdot(k\nabla T) + \lambda\Psi + \mu\Phi + \dot{Q} \quad (14)$$

$$\Psi = \left(\frac{\partial u}{\partial x} + \frac{\partial v}{\partial y} + \frac{\partial w}{\partial z}\right)^2 \quad (15)$$

$$\Phi = 2\left[\left(\frac{\partial u}{\partial x}\right)^2 + \left(\frac{\partial v}{\partial y}\right)^2 + \left(\frac{\partial w}{\partial z}\right)^2\right] + (\frac{\partial u}{\partial y} + \frac{\partial v}{\partial x})^2 + (\frac{\partial v}{\partial z} + \frac{\partial w}{\partial y})^2 + (\frac{\partial w}{\partial x} + \frac{\partial u}{\partial z})^2 \quad (16)$$

where $\vec{f}$ is the body force, k is the thermal conductivity, c_p is the specific heat of gas, μ dynamics viscosity, λ is bulk viscosity, $\vec{U}$ is the velocity vector, and u, v, and w represent the velocity magnitude in each of the three Cartesian directions.

During experiments, the microreactor wall is heated to temperatures between 1300-1700 K. The carrier gas, which is typically at room temperature at the inlet, experiences a dramatic temperature change within the short residence time of the reactor. Thus, valid thermodynamic functions for the thermal conductivity and dynamic viscosity of Helium are necessary to obtain reliable simulation results. These parameters have been previously determined experimentally and are adapted as follows[33],

[33] Petersen, Helge. The properties of helium: density, specific heats, viscosity, and

$$k = 2.682 \cdot 10^{-3}(1 + 1.123 \cdot 10^{-3}P)T^{\left(0.71\left(1-2\cdot 10^{-4}P\right)\right)}\ [W/(m * K)] \quad (17)$$

$$\mu = 3.67\times 10^{-7} \cdot T^{0.7}\ [Pa.s] \quad (18)$$

where T and P have units of Kelvin and Bar respectively.

This system of equations has been implemented using ANSYS Fluent and MATLAB. Fluent is a commercial CFD software package used for simulating complex fluid flows in a large range of applicable cases from uncompressible to highly-compressible flow[34]. It can achieve the highest convergence speed and solution accuracy among current CFD software through the implementation of multiple solution methods and different structured girds. Fluent can solve various engineering problems including turbulence, heat transfer and phase-change, reaction flow, multiple-phase flow, and turbomachinery. Nowadays, ANSYS Fluent occupies more than 60% of the market share and is widely applied in U.S industries like aerospace engineering, vehicle design, and petroleum and natural gas development.

---

thermal conductivity at pressures from 1 to 100 bars and from room temperature to about 1800 K. 1970.

[34] Fluent, A. N. S. Y. S. "Ansys fluent theory guide." ANSYS Inc., USA 15317 (2011): 724-746.

Three dimensional models of reactors with different structure parameters were built in ICEM[35] using a tetrahedral mesh. Structured tetrahedral mesh is a general mesh style for three dimensional models' discretization. It is suitable for a large number of model profiles, while being easy to build with a low probability of error with respect to structural geometry. Compared to a hexahedral mesh, models with tetrahedral mesh have a relatively high speed of convergence, even though, as a disadvantage, they are less accurate in terms of simulation results. To study the microreactor design numerically, models with different structure parameters need to be built and calculated in a short amount of time. The relatively simple profiles of the models reduce the impact of mesh shape on the simulation accuracy, which is why a tetrahedral mesh is selected.

The density-based solver was applied with the SIMPLE scheme[36,37] using a second-order-upwind discretization method. The density-based solver couples equation groups that can solve the continuity, momentum, energy and species transport equations simultaneously. For high-speed compressible flow, the density-based solver typically requires a lower

[35] ANSYS, ICEM CFD. "13: geometry and mesh generation preprocessor." Ansys Inc.

[36] Ambatipudi, Vaidehi. "SIMPLE Solver for Driven Cavity Flow Problem." Department of Mechanical Engineering, Purdue University (2010).

[37] Mangani, L., and C. Bianchini. "Heat transfer applications in turbomachinery." Proceedings of the OpenFOAM International Conference. 2007.

number of iterations to reach convergence than pressure-based solvers. The SIMPLE scheme is a numerical procedure widely applied to solve Navier-Stokes equations for uncompressible flow and was first proposed in 1972. It fundamentally supposes that the velocity field and assumed pressure field operate independently (do not influence each other), and that the correction to the pressure field is obtained from solutions of the mass conversation equation for the velocity field. The revised algorithm[38] was presented in 1979, which allowed the initial velocity and pressure fields to be assumed independently to extend the application of the SIMPLE method to compressible flow.

3.2 PIMS Experimental Methods

The performance testing of the novel reactor prototype is conducted using the PIMS system, which has been discussed in the previous chapter and is briefly summarized here. As shown in Figure 6, the biofuel reactants ($\leqslant$0.1 mol%) mixed with carrier gas, He, are injected into a heated microreactor. The reactions happen inside the tube over very short residence times ($50\sim200\ \mu s$) and are then suddenly arrested upon exiting the microreactor, where the flow forms a supersonic jet. The products travel to the downstream vacuum chamber, where pressure is stabilized at 1×10^{-6} Torr

[38] Tannehill, John C., Dale A. Anderson, and Richard H. Pletcher. "Computational fluid mechanics and heat transfer, Series in computational and physical processes in mechanics and thermal sciences." (1997).

by a Varian VHS-6 diffusion pump. The products are then ionized by 30Hz vacuum ultraviolet (VUV) radiation (generated by a Spectra-physics Nd: YAG laser). An electrical field is imposed in the Z-direction, causing the ionized products to fly up to the Jordan reflection time-of-flight spectrometer, where they are detected. The mass spectrometer typically collects more than 1000 scans to average with a $\Delta m/m$ resolution around 400. Differing from the IR setup, the PIMS system can obtain results in approximately 10 mins for every individual experiment, significantly reducing experimental time.

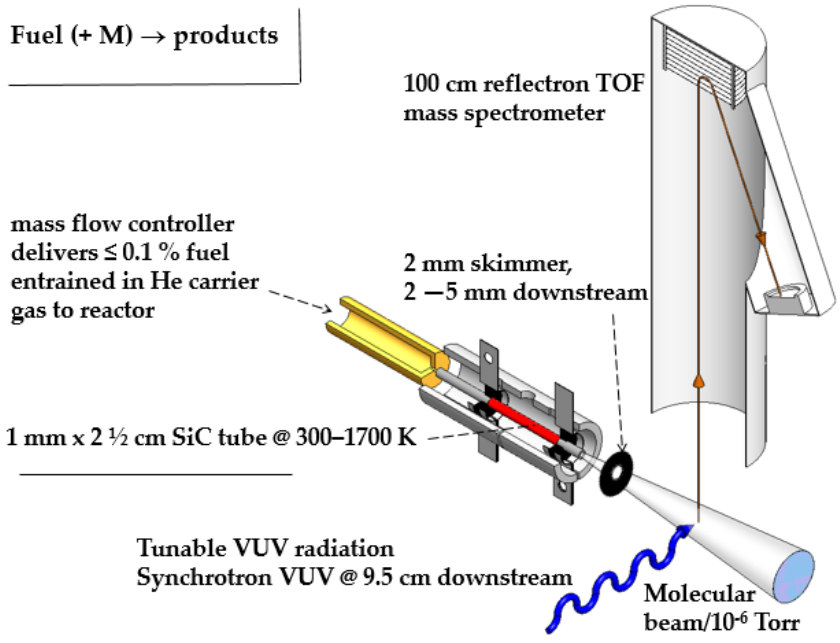

Figure 6: Schematic of the photoionization mass spectrometry system

The reactor's wall temperature is record by an Omega C-Type thermocouple and can be adjusted by a 100 W manual electric heater to run experiments

at different fixed temperatures. The current Silicon Carbide (SiC) reactor cannot withstand a temperature higher than 1600 K, and therefore 1600 K is the upper limit on experimental temperatures. The pulsed valve fires at a frequency of 30 Hz and is open for approximately 100 μs. According to experimental evaluation, we know that the average mass flow rate is about 9.9 SCCM, which was found by calculating the upstream pressure gauge reading change. This means the actual mass flow rate during every pulse is around 300 SCCM.

To verify CFD simulation results by experiments, we first fabricated a novel reactor prototype, which has structure parameters L = 28 mm, d = 0.5 mm and G1 = 0.8 mm (for details, see Chapter 4). Two experiments are proposed to test the performance of the new reactor, one of which involves propionaldehyde decomposition, which has been previously researched[39]. We seek to repeat the propionaldehyde experiments that we know work with the old reactor to ensure reproducibility and to verify that there have been no changes in chemicals or operating conditions that may account for changes in results. Theoretically, products including CH_3, CH_2CH_2 and CH_3CCH should be discovered in the temperature range of 1400-1600 K as was observed in the prior experiments. Then we will repeat the

[39] Warner, Brian J., et al. "Products from Pyrolysis of Gas-Phase Propionaldehyde." The Journal of Physical Chemistry A 119.1 (2014): 14-23.

propionaldehyde experiments using the new reactor prototype to compare with the old data and make sure there are no obvious changes. Propionaldehyde is an appropriate sample because there is possibility of secondary reactions, which would be enhanced with higher pressures so varied reactor pressure may influence product distributions if bimolecular reactions play an important role.

For the second set of proposed experiments, a well-known "chemical thermometer"[40-42] cyclohexene, is used to judge the differences between the internal flow in classical reactors and the novel microreactor prototype. Under high temperature, cyclohexene will decompose to ethylene and butadiene. The rate of this reaction is highly-dependent on temperature and pressure; therefore, we expect to obtain different degrees of reaction process between two reactors by analyzing the products, demonstrating the differences in thermal properties of each reactor.

---

[40] Tranter, R. S., et al. "Calibration of reaction temperatures in a very high-pressure shock tube using chemical thermometers." International Journal of Chemical Kinetics 33.11 (2001): 722-731.

[41] Heyne, Joshua S., and Frederick L. Dryer. "Uncertainty analysis in the use of chemical thermometry: A case study with cyclohexene." The Journal of Physical Chemistry A 117.26 (2013): 5401-5406.

[42] Kiefer, John H., and Jatin N. Shah. "Unimolecular dissociation of cyclohexene at extremely high temperatures: behavior of the energy-transfer collision efficiency." J. Phys. Chem.;(United States) 91.11 (1987).

CHAPTER 4

RESULTS

4.1 CFD Design Results

4.1.1 Influence of the Choke Diameter, d

The influence of the choke diameter, d, on the microreactor center line pressure and velocity profiles was determined for several inlet mass flow rates. The choke diameter was varied from 0.10 to 0.30 mm, while holding all other geometric variables constant (L = 21 mm, G1 = 3 mm, and G2 = 2 mm). The results seen in Fig. 7 through Fig. 10 demonstrate that without the nozzle structure, the pressure profile continuously decreases from the inlet pressure to zero along the length of the reactor. Upon addition of the nozzle structure, it is shown the pressure distribution becomes stable within the main body of the microreactor, and the maximum center line pressure is directly affected by changing the choke diameter, d. Similarly, the calculated Mach number profiles plateau within the microreactor main body with the addition of the nozzle structure. Therefore, we can design the new microreactor to have specific pressure and Mach number conditions simply by tuning the choke diameter for a desired inlet flow rate.

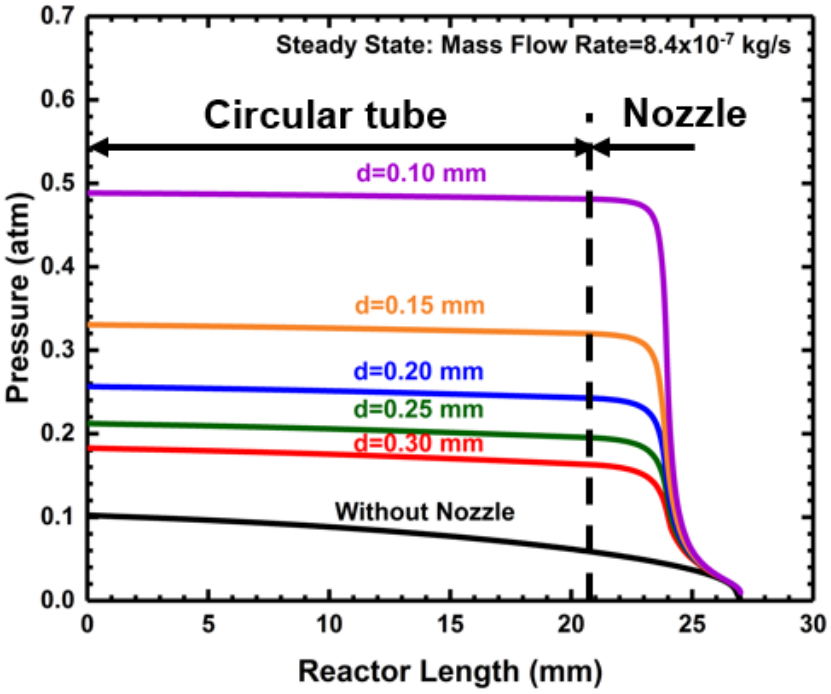

Figure 7: Center line pressure distribution for various choke diameters d.

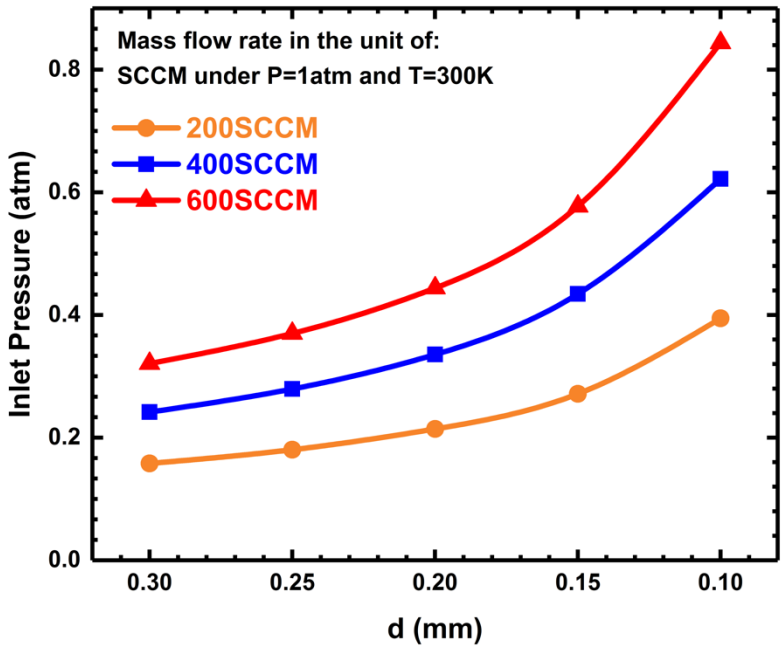

Figure 8: Micro-reactor inlet pressure as a function of choke diameter, d, for various inlet flow rates.

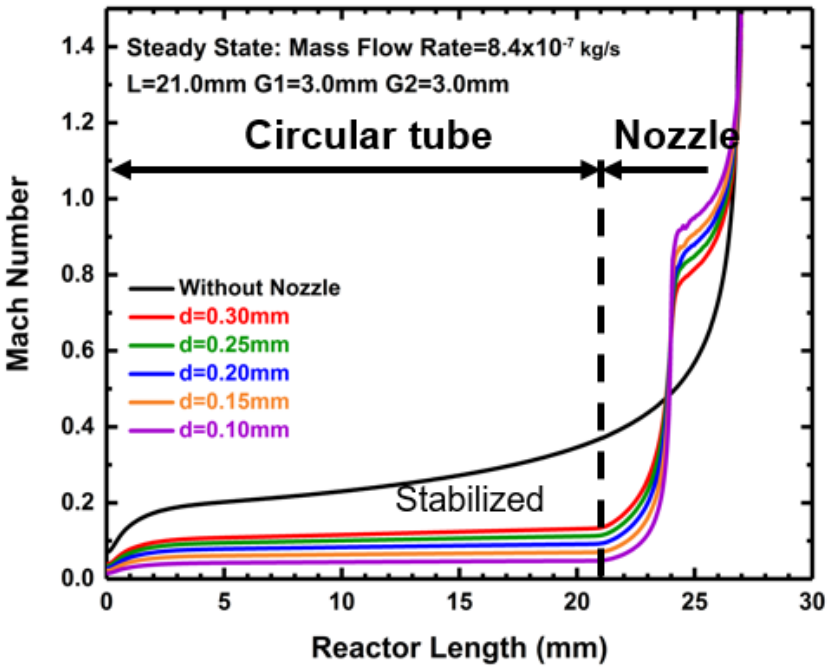

Figure 9: Central line Mach number distribution along the reactor length for various choke diameters, d.

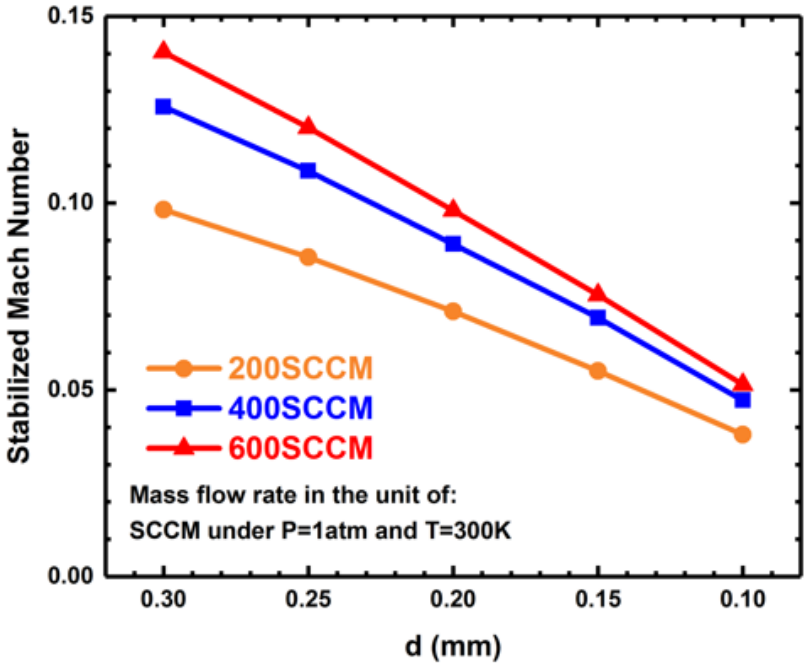

Figure 10: Micro-reactor stabilized Mach number as a function of choke diameter, d, for various flow rates.

4.1.2 Influence of G1 & G2 and L

Further calculations were carried out to determine the influence of the lengths of both the converging and diverging nozzles, G1 and G2 respectively. The simulation results for the center line pressure profiles along the nozzle length are depicted in the Fig. 11 and Fig. 12. When the converging nozzle length, G1, increases from 3.0 mm to 5.0 mm, the inlet pressure only changes by ~0.02 atm, which is negligible. The converging nozzle length, G1, also has negligible effects on predicted velocity and residence time, demonstrating that the ideal converging nozzle length for our microreactor is that which is easiest to fabricate. The same conclusions may be drawn for adjusting the diverging nozzle length, G2. We have decided to remove the diverging nozzle structure because of its negligible effects on the properties of the new microreactor other than to increase fabrication difficulty.

Finally, simulations were conducted where the microreactor main body length, L, was varied from 20 to 30 mm. These results showed that by increasing the reactor length, the only significant property change observed was an increase in residence time.

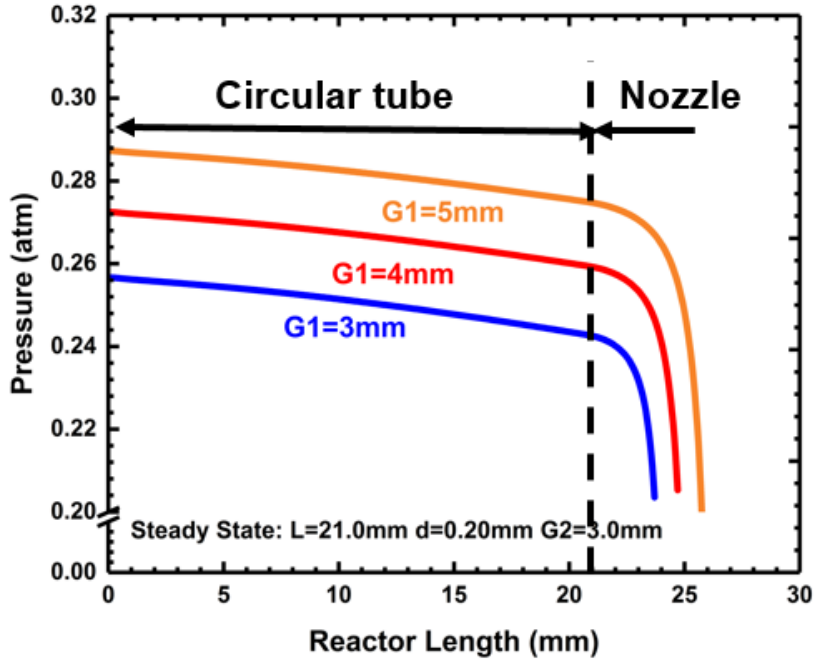

Figure 11: Pressure distribution along as a function of reactor length for various converging nozzle lengths, G1.

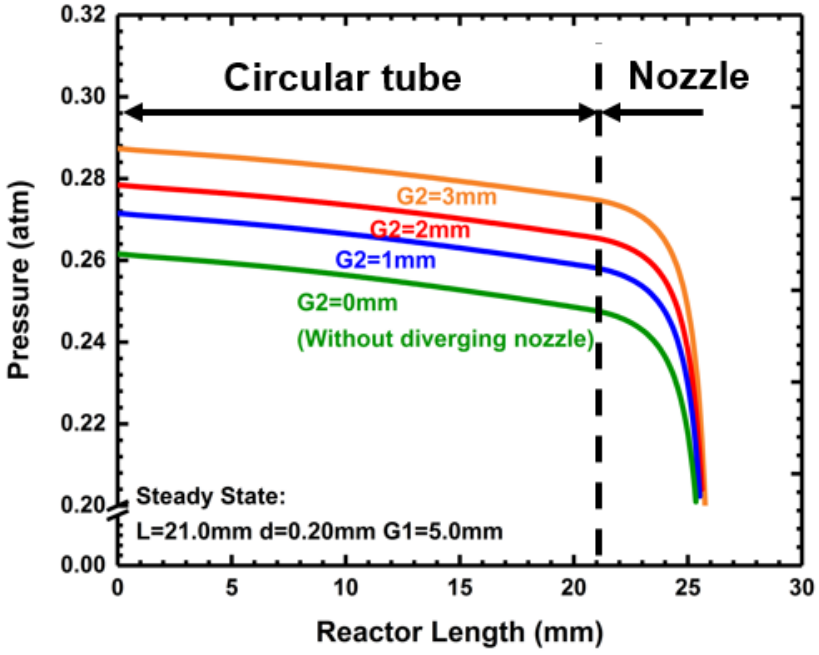

Figure 12: Pressure distribution along as a function of reactor length for various diverging nozzle lengths G2.

4.1.3 Thermodynamics Profiles of the Redesigned Reactor versus the Chen Nozzle

As a result of the previously described simulations, we have identified preliminary design specifications for the new microreactor system (L = 20 mm, G1 = 5 mm, d = 0.15 mm). To directly compare the calculated performance of the new system to the existing system, we have directly compared the calculated pressure, velocity, temperature, and Knudsen number profiles in Fig. 13 and Fig. 14 using an inlet flow rate of 300 SCCM. The Knudsen number is a dimensionless parameter which determines whether statistical mechanics or continuum mechanics should be used for fluid dynamics modeling (see Eqn. 19).

$$Kn = \frac{\lambda}{D} = 1.26\sqrt{\gamma}\frac{Ma}{Re_D} \tag{19}$$

where λ is the molecular mean free path and Ma is the Mach number. Typically, when the Knudsen number is less than 0.1, the Navier-Stokes equation is applicable[43].

In Fig. 13, the simulation results show that at the center line of the redesigned reactor, the pressure and velocity profiles remain stable and the

[43] Bird, Graeme Austin. "Molecular gas dynamics." *NASA STI/Recon Technical Report A* 76 (1976).

maximum temperature is reached at ~6 mm down the length of the reactor. It is also observed that the design changes had minimal impact on the temperature distribution within the reactor. It is important to mention that the Knudsen number, in both cases, remains less than 0.1, which suggests that the Navier-Stokes equation was appropriate for modeling this system. The impact of the microreactor structure parameters on the thermodynamics profiles are shown in Table 1. Choke diameter, d, has the greatest effect on the fluid properties within the microreactor, while changing the nozzle lengths G1 and G2 had negligible effects. Varying the microreactor length, L, had little influence on pressure, temperature, and velocity, but had a direct influence on predicted residence time.

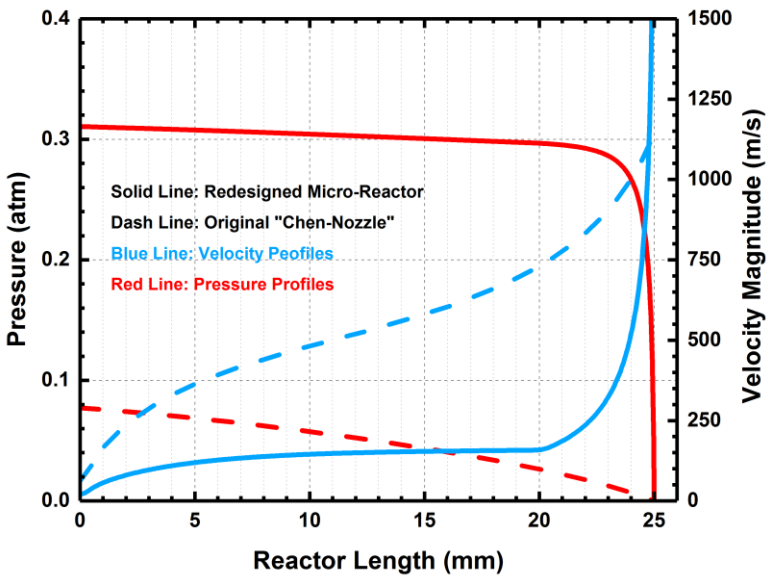

Figure 13: Center line pressure and velocity distribution along with the reactor of both redesigned micro-reactor and original reactor

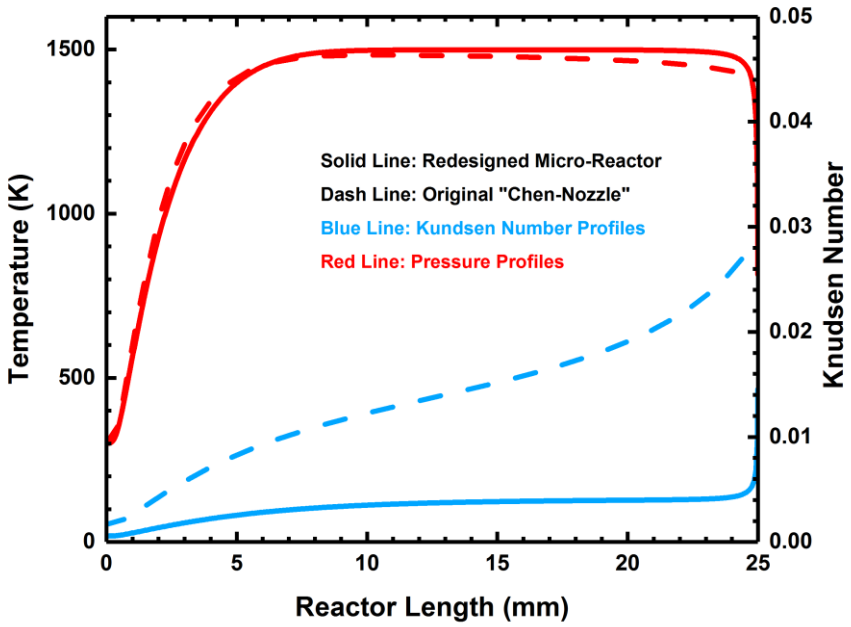

Figure 14: Center line temperature and Knudsen number distribution along with the reactor of both redesigned micro-reactor and original "Chen nozzle"

	Pressure	Velocity	Temperature	Residence time
d	●	●	○	●
G1	◐	◐	○	◐
L	○	○	○	●

● **Distinct Influence** ◐ **Slight Influence** ○ **Almost No Influence**

Table 1: The influence of reactor structure parameters on thermodynamics profiles

4.1.4 The Necessity of Continuous Reaction Flow

At the University of Colorado Boulder, continuous flow conditions are not able to be achieved due to restrictions in pumping capacity. Instead, the experiment operates at pulsed conditions. To reflect the realistic conditions of the current experimental operation, 3D-transient models (L = 20 mm, G1 = 5 mm, d = 0.20 mm) have been performed to compare the thermodynamic environments in the reactors between "pulse flow" and continuous flow. In the simulation, the pulse valve open time is set to 1.0 to 2.0 ms and has a constant frequency of 30 Hz, which is based on experimental values. Prior to opening the pulsed valve, the pressure inside the reactor system is nearly a vacuum.

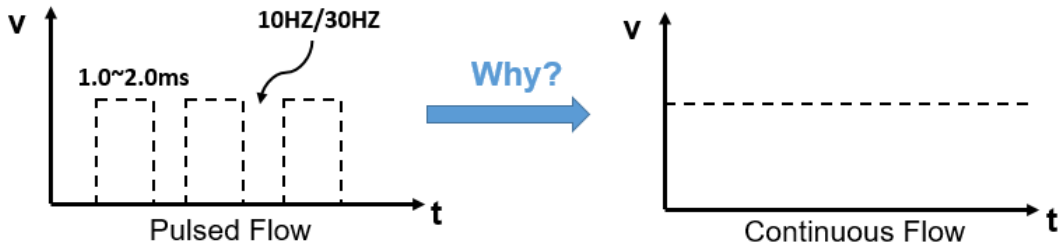

Figure 15: Rection flow supply diagram of plused flow and continous flow

According to the results shown in Fig. 16 and Fig. 17, the pressure profiles experience a sudden increase and then quickly decrease from the valve opening to the end of every pulse. Due to these pulses, the pressure profiles do not reach steady state. The pulsing also affects the temperature profiles,

hindering the temperature from reaching wall temperature. These are unacceptable to correctly study the chemical kinetics of a system. Therefore, achieving continuous flow conditions in the experiment is a primary objective for system improvements, which can be realized by installing a more powerful turbo pump to replace the current diffusion pump.

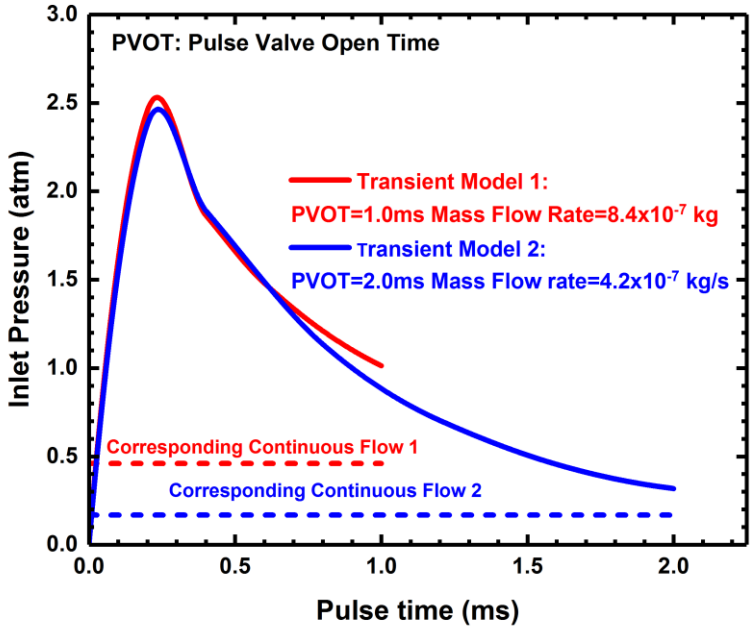

Figure 16: Inlet pressure change with pulse time during "pulused flow" and the corresponding continuous flow. (Red line indicate PVOT = 1.0ms, Blue line indicate PVOT = 2.0ms, PVOT = pulsed value opem time)

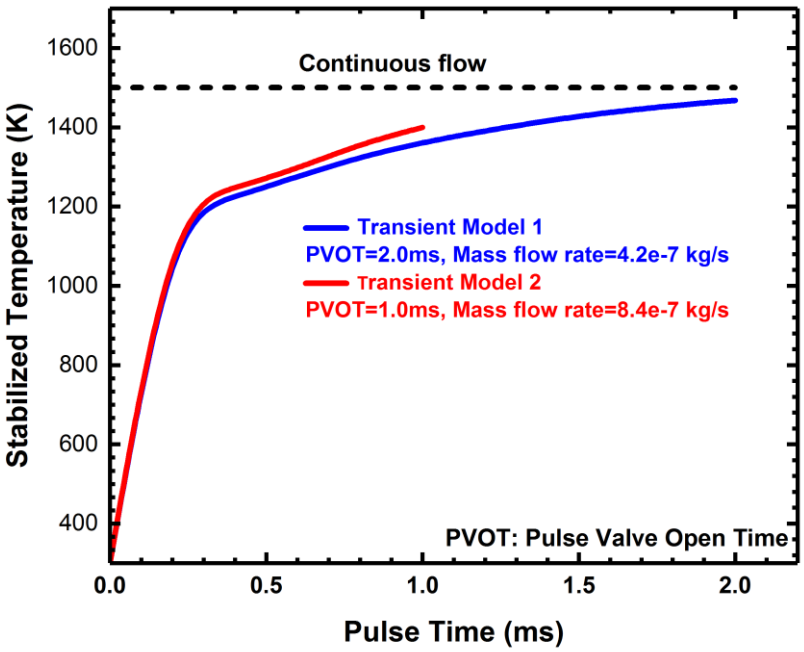

Figure 17: Stabilized temperature change with pulse time during "pulsed flow" and the corresponding continuous flow

4.1.5 The Influence of Helium Thermal Properties Uncertainty

The thermal properties of carrier gases, such as thermal conductivity and dynamic viscosity, help determine internal flow conditions and heat transfer efficiencies in the microreactor. Qi and Daily in Ref. [30] proved there is a distinct difference in the predicted thermodynamic profiles for microreactors when injected with Helium versus Argon. Similarly, the uncertainties associated with the experimental formula, Eq. 20 and 21, for thermal properties of Helium may lead to considerable errors in calculation results.

$$k = 2.682 \cdot 10^{-3}(1 + 1.123 \cdot 10^{-3}P)T^{\left(0.71\left(1-2\cdot 10^{-4}P\right)\right)}\ [W/(m * K)] \qquad (20)$$

$$\mu = 3.67\times 10^{-7} \cdot T^{0.7}\ [Pa.s] \qquad (21)$$

Therefore, a 20% error range is assigned to the Helium thermal property formulas, where thermal conductivity and dynamics viscosity are varied by +/- 20% and substituted back into the CFD simulations to investigate the influence of possible errors on the predicted pressure and temperature profiles. The calculation is implemented in a reactor model with the structure parameters of L = 20 mm, G1 = 5 mm, and d = 0.25 mm. The steady state mass flow rate is 300 SCCM and wall temperature is 1500 K. The results, shown in Fig. 18 and Fig. 19, demonstrate how the uncertainties associated with the thermal conductivity directly influence the predicted distance at which the center line temperature profile reaches the wall temperature, and how a larger dynamic viscosity may lead to higher inlet pressure. Fortunately, the impacts of the uncertainties in He thermal parameters are within an acceptable range when compared with the influence of structural parameters on the simulations.

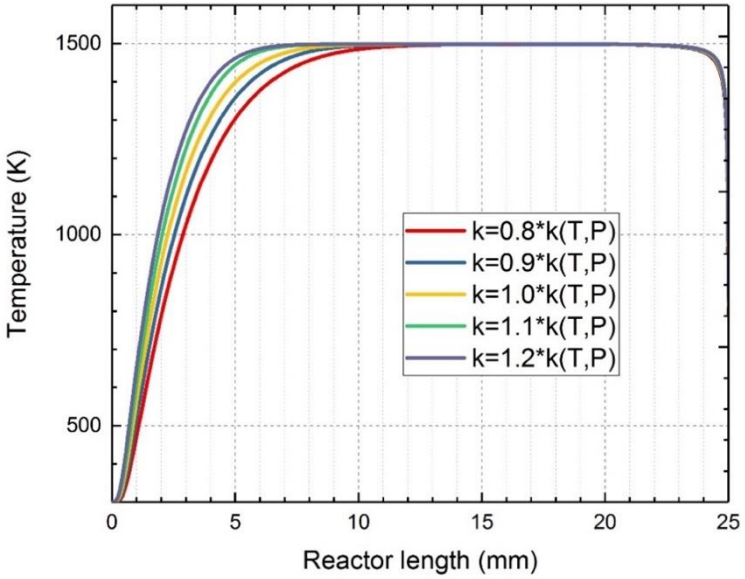

Figure 18: The influence of helium thermal conductivity uncertainty on center line temperature distributions

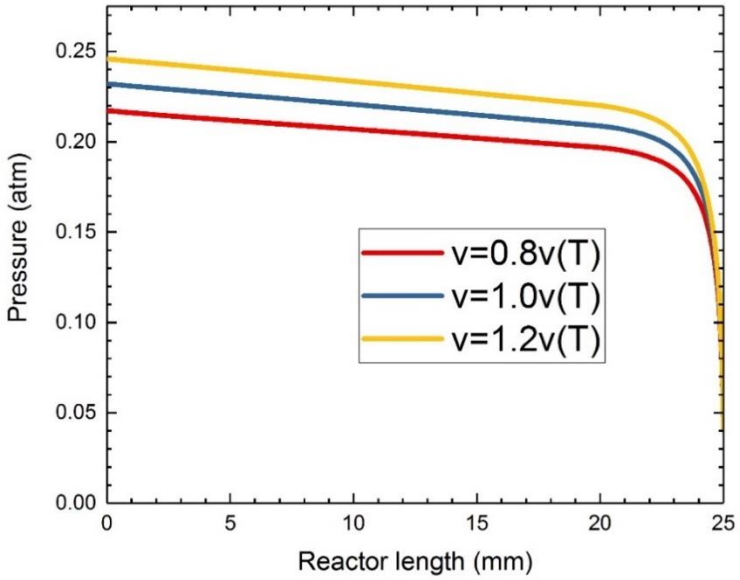

Figure 19: The influence of helium dynamic viscosity uncertainty on center line pressure distributions

4.1.6 Micro-reactor Radial Profiles

As a complement of the above results, we also provide radial velocity and temperature profiles for the L = 21 mm, d = 0.15 mm, G1 = 5 mm, SCCM = 300 calculation case in Fig. 20 and Fig. 21. According to the results, the radial velocity profiles decrease from center line to the reactor wall due to viscous fluid boundary layer effects. Also, the magnitude of the difference between the center line temperature and the wall temperature depend on the positions of reactor length.

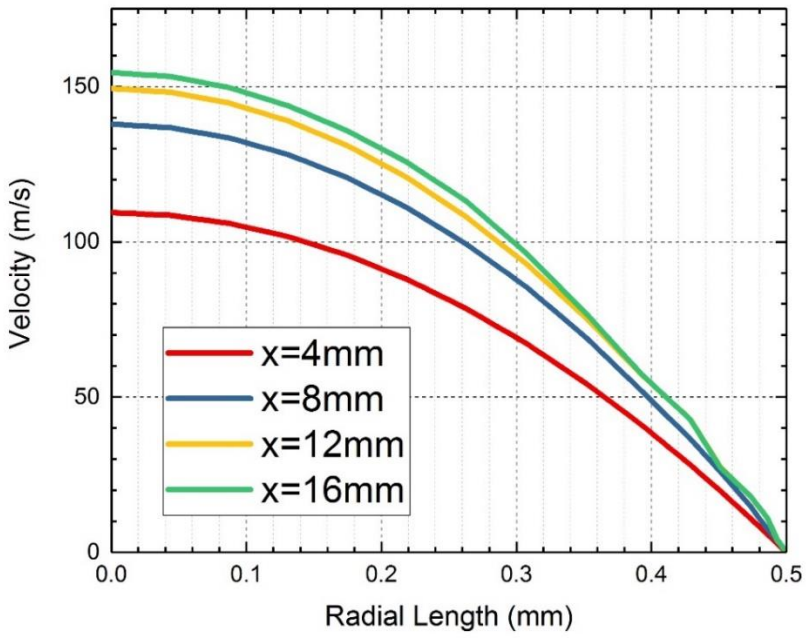

Figure 20: Velocity radial profiles at reactor inlet length X = 4 mm, 8 mm, 12 mm, and 16 mm.

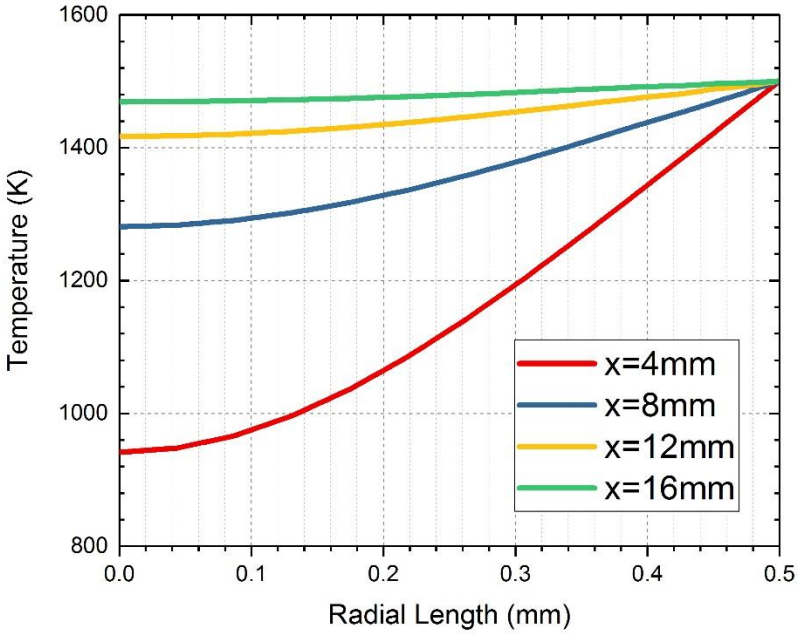

Figure 21: Temperature radial profiles at reactor inlet length X = 4 mm, 8 mm, 12 mm, and 16 mm.

4.2 Microreactor Materials Research for Oxidation Reaction

The current rector material silicon carbide (SiC) is a carborundum ceramic that has high thermal stability and acid-base corrosion resistance. However, silicon carbide corrodes in oxygen atmosphere under high temperature. The key reaction is shown below:

$$\mathrm{SiC} + O_2 \rightarrow SiO + CO \qquad (22)$$

As a result, the experiments with the current microreactor are limited to pyrolysis (thermal decomposition in the absence of oxygen). To carry out

combustion reactions of biofuels in the current PIMS system, we must identify a new material for the reactor. The microreactor material should be chemically inert in an oxidizing atmosphere and structurally sound over a temperature range of 300 to 2000 K. Here we present some explored alternative materials for the new microreactor.

4.2.1 Non-metal Materials

For non-metal materials, some specialty ceramics may satisfy our materials requirements. We first explored other ceramics including silicon nitride (Si_3N_4). Similar to silicon carbide, silicon nitride will also oxide around a temperature of 1600 K, even though its oxidation reaction rate is much slower than that of silicon carbide[44]. The oxidation reaction is given by:

$$Si_3N_4 + 3O_2 \rightarrow 3SiO_2 + 2N_2 \quad (23)$$

Engineered alumina ceramics ($Al_2O_3 + SiO_2$) may be a good choice for our reactor since it does not react with oxygen and has a high melting point, exceeding 2000 K. One drawback is its weak thermal shock resistance. When the operation temperature suddenly changes, alumina ceramics can

[44] Munro, R. G., and S. J. Dapkunas. "Corrosion characteristics of silicon carbide and silicon nitride." *Journal of research of the National Institute of Standards and Technology* 98.5 (1993): 607.

crack because of its brittle structure[45]. Further research is required to determine if an engineered alumina ceramic would be a valid material for our reactor. Other oxide ceramic candidates include MgO[46] and ZrO_2[47], which nowadays are widely used to fabricate gas turbine blades. Composite ceramics may also be applicable. Here, we provide a table to summarize the above ceramics properties from Ref. [45] to Ref. [48]:

Materials Name	Melting Point (K)	Thermal Conductivity (W/m*K)	Thermal Expansion (10^{-6}/K)	Thermal Shock Resistance (Water Immersion Testing)	Electrical Resistivity (Ohm*m)	Reactivity with Oxygen
SiC	~1950	3.8~20.7	7.9~11	400	10^1~10^4	Reactive
Si_3N_4	~2750	10~43	1.4~3.7	550	10^8~10^{13}	Reactive
Al_2O_3	~2350	12~38.5	4.5~10.9	200	10^{10}~10^{14}	Non-Reactive
MgO	~3100	30~60	9.0~12.0	–	10^{12}~10^{13}	Non-Reactive
ZrO_2	~2850	1.7~2.7	2.3~12.2	300	10^5~10^{10}	Non-Reactive

Table 2: Thermal properties and reactivity of common high-temperature ceramics materials. (Data from Ref. [45] to Ref. [48])

4.2.2 Metal Materials and its Coating Technology

Metal or alloy materials should also be considered for their high melting point, high thermal shock resistance, and low cost. They can not only be used for the current oxidation set up, but also for future experiments

[45] Auerkari, Pertti. *Mechanical and physical properties of engineering alumina ceramics*. Espoo: Technical Research Centre of Finland, 1996.

[46] Shand, Mark A. *The chemistry and technology of magnesia*. John Wiley & Sons, 2006.

[47] Nielsen, Ralph. "Zirconium and zirconium compounds." *Ullmann's Encyclopedia of Industrial Chemistry* (2000).

involving biofuel reactions in acidic or alkaline environments. Here, we provide thermal properties and reactivity for several common metals[48-52] in Table 3, where most metals are reactive for hyperthermal oxidation. Besides, the novel metals, gold and platinum, possibly react with organics biofuels[53,54], even though are stable in an oxygenated atmosphere.

Materials Name	Melting Point (K)	Thermal Conductivity (W/m*K)	Thermal Expansion (10^{-6}/K)	Electrical Resistivity (Ohm*nm)	Reactivity
Stainless Steel 304	~1720	14~17	16~18	650~770	Hyperthermal Oxidation
Titanium	~2000	~17	~8.6	~420	Hyperthermal Oxidation
Tungsten	~3670	170~175	4.2~4.6	54~60	Hyperthermal Oxidation
Gold	~1338	305~319	13.5~14.5	20~30	Organogold
Platinum	~2050	70~72	9~9.2	104~108	Organoplatinum

Table 3: Thermal properties and reactivity of common metal materials. (Data from Ref. [49] to Ref. [55])

Since most metals or alloys are conductive and hard to heat electrically, we

[48] Rose, Lars. *On the degradation of porous stainless steel in low and intermediate temperature solid oxide fuel cell support materials*. Diss. University of British Columbia, 2011.

[49] "Titanium". *Columbia Encyclopedia (6th ed.). New York:* Columbia University Press. *2000–2006.* ISBN 0-7876-5015-3. *Archived from the original on 18 November 2011.*

[50] Walsh, Patrick N., Jean M. Quets, and Robert A. Graff. "Kinetics of the Oxygen—Tungsten Reaction at High Temperatures." *The Journal of Chemical Physics* 46.3 (1967): 1144-1153.

[51] Kelly, P.F. (2015). *Properties of Materials*. CRC Press. p. 355. ISBN 978-1-4822-0624-1.

[52] Weast, Robert (1984). *CRC, Handbook of Chemistry and Physics*. Boca Raton, Florida: Chemical Rubber Company Publishing. pp. E110. ISBN 0-8493-0464-4.

[53] Parish, R. V. "Organogold chemistry: II reactions." *Gold Bulletin*30.2 (1997): 55-62.

[54] Nickel, *Palladium and Platinum (Comprehensive Organometallic Chemistry II)* R.J. Puddephatt (Editor) 2002 0080423167

cannot directly use metals to fabricate our reactor. Alternatively, coating technologies are needed to cover metal materials on the inner wall of non-metal reactors. Instead of traditional galvanization method, we here present another possibly suitable technology – sputter coating.

Sputter coating is a physical vapor deposition (PVD) method of thin film deposition, especially appropriate for coating high melting point metals[55]. A schematic of a microreactor being coated using the sputtering coating process is shown in Fig. 22. In this process, a target metal micro-wire is inserted into (not touching) the reactor substrate, and a high voltage electric is imposed from a substrate anode to target cathode in an Argon atmosphere. Argons atoms are ionized under a high electric field and the ions then fly to the cathode target, where metal atoms activated by absorbing argon ions. Once activated, the metal atoms re-emit to the reactor substrate and finally deposit on its surface.

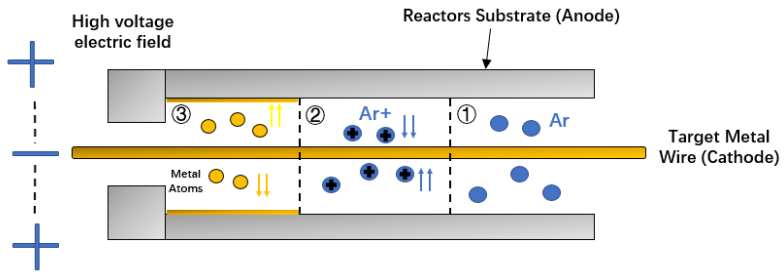

Figure 22: The protray of micro-reactors sputtering coating process

[55] Echlin, P. "Sputter coating techniques for scanning electron microscopy." *Scanning Electron Microsc* 2 (1975): 217-224.

The above machine process can be implemented using instruments from Joint Institute for Laboratory Astrophysics (JILA) at the University of Colorado Boulder. Limitations of this method include expense and time for manufacturing.

4.3 Experimental Procedures for Testing the Microreactor Prototype

4.3.1 Initial Prototype of Novel Microreactor

A novel reactor prototype was fabricated by silicon carbide, whose structure is shown in Fig. 23.

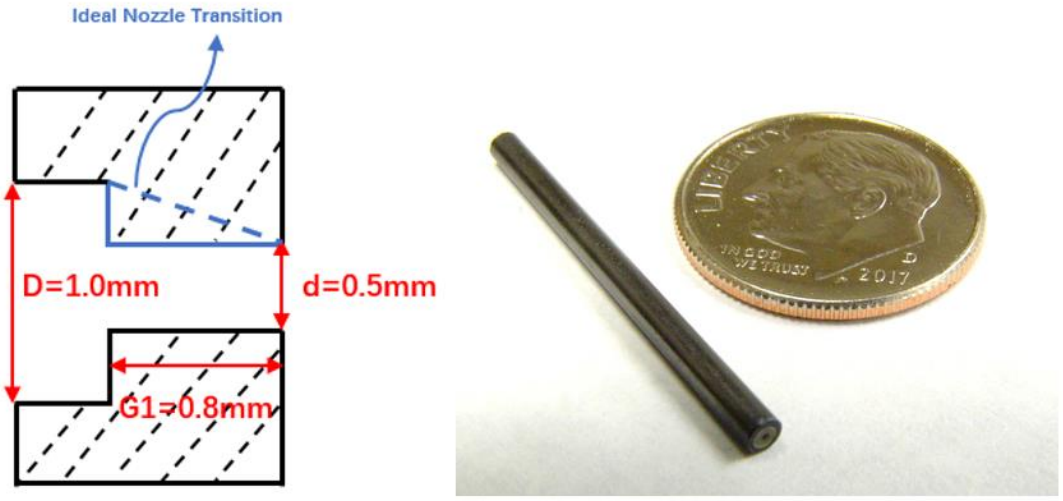

Figure 23. A photo and structure diagram of the novel reactor prototype

The main body diameter is kept at 1.0 mm and the main body length is kept at 28 mm to be consistent with the original microreactor. The nozzle was constructed by inserting a 1 mm outer diameter, 0.5 mm inner diameter,

0.8 mm long piece of alumina ceramic tubing into the existing 1.0 mm inner diameter silicon carbide tube. The result is a microreactor with a built in rectangular plug nozzle structure, which is different in geometry when compared to the angled shape of the ideal nozzle, which is shown in Fig. 22 as the blue dashed line. This microreactor, as well as the previous reactors, have been fabricated at the CIRES (Cooperative Institute for Research in Environmental Science) machine shop by Don David. Even though the prototype structure has design elements different than our final reactor design, we have gone forward on building this low cost and rapidly machined version to conduct proof of concept experiments for the time being before pursuing more expensive fabrications of the reactor. Here, we also provide pressure, velocity and temperature distributions of that novel prototype, as shown in Fig. 24 and Fig. 25 following.

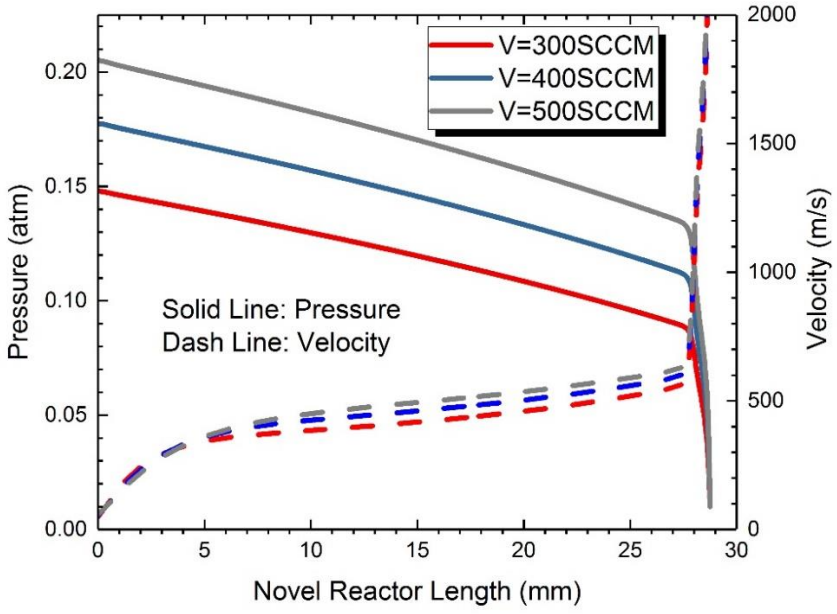

Figure 24: Center line pressure and velocity profiles of the fabricated novel reactor prototype shown in Fig. 23 under different mass flow rates

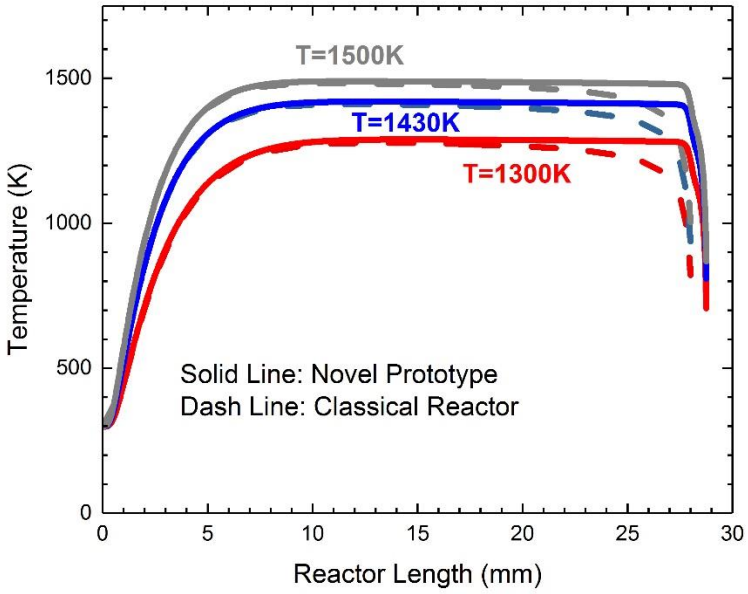

Figure 25: Center line temperature profiles of the novel prototype shown in Fig. 23 and the classical reactor (mass flow rate V=300 SCCM)

4.3.2 Completed Propionaldehyde Verification Experiments

As shown in Fig. 26, a pyrolysis reaction experiment was performed for samples of 0.07% propionaldehyde in helium, and the products were ionized at 10.5 eV. The mass spectra results obtained similar products to the original data set obtained under the same experimental conditions in 2014 (shown in Fig. 27), which helps validate the effectiveness of the PIMS system. The products include CH_3, CH_2CH_2, $CH_3C \equiv CH$, and methyl-ketene.

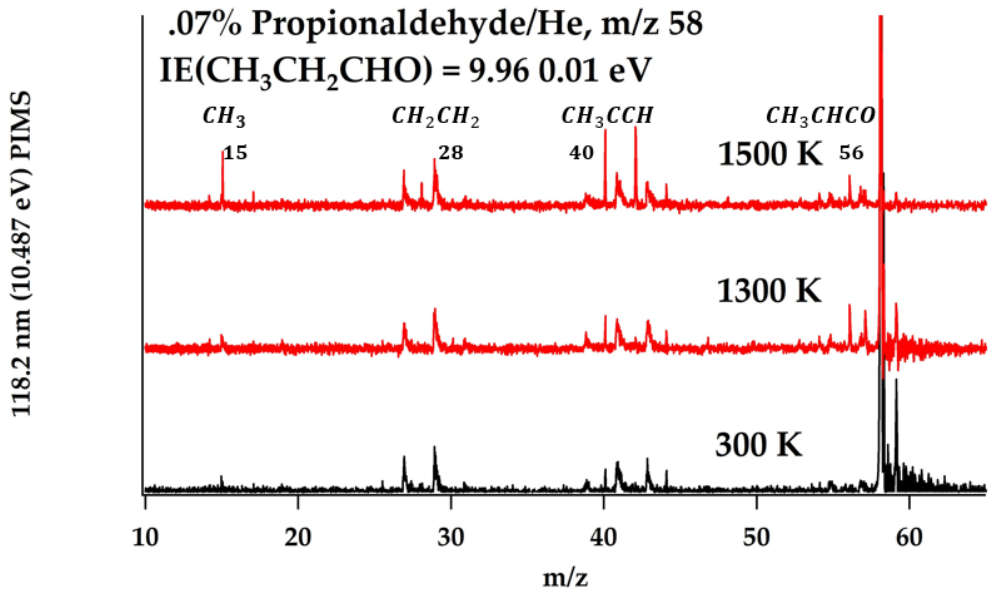

Figure 26. Current mass spectra of 0.07% propionaldehyde/He at 300 K, 1300 K, and 1500 K in 2017.

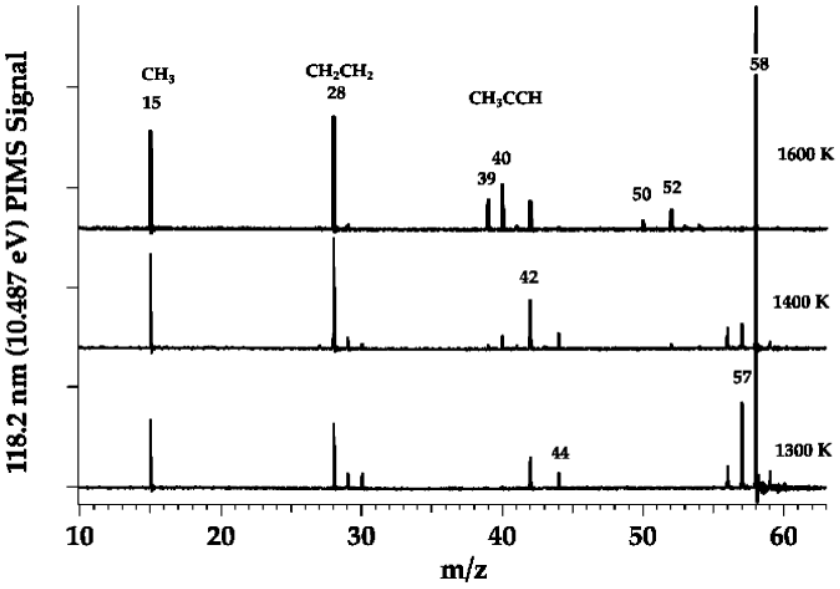

Figure 27. Original mass spectra of 0.3% propionaldehyde/He at 10.5 eV at 1300 K, 1400 K, and 1600 K from Ref. [41] in 2014.

From the mass spectra results we can determine the four main paths of propionaldehyde pyrolysis present for this experiment (for detailed investigations and explanations, see Ref. [41]). The pathways are an $\alpha - C - C$ bond scission reaction,

$$CH_3CH_2CHO + (M) \rightarrow CH_3CH_2 + HCO \quad (24)$$

a $\beta - C - C$ bond scission reaction,

$$CH_3CH_2CHO + (M) \rightarrow CH_3 + CH_2CHO \quad (25)$$

and two elimination/isomerization reactions.

$$CH_3CH_2CHO + (M) \rightarrow CH_3CH = C = O + H_2 \quad (26)$$

$$CH_3CH_2CHO + (M) \rightarrow CH_3C \equiv CH + H_2O \quad (27)$$

It is important to note other products not observed by the above mass spectra might be exhausted by secondary reactions or the ionization threshold of the molecules may be above the energy of our laser.

Some disturbances and noise are found in the current mass spectra as compared to the previous spectra. This suggests that the system needs further adjustments to be completed before further experiments can be continued. At the time of this thesis, these adjustments were not completed in time and so here we outline a detailed experimental procedure for further testing of the reactor prototype.

4.3.3 Proposed Propionaldehyde Verification Experiments

Propionaldehyde decomposition experiments will also be carried out in the novel reactor prototype using same experimental settings to distinguish thermal environment differences between classical reactors and novel prototypes. There is some evidence that bimolecular chemistry plays a role in the propionaldehyde experiments. If so, we would expect to see some different products produced by the two different reactors in the experiments. However, we would expect that the two different reactors, should bimolecular reactions not play a significant role, would produce the same product distribution.

4.3.4 Cyclohexene Experiments Design and Predictions

To further distinguish the performance of the prototype from the classical reactor, we plan to conduct experiments with cyclohexene, a “chemical

thermometer", since the reaction in Eqn. 28 is well researched previously[56]. Through the following reaction,

$$c - C_6H_{10} \rightarrow C_4H_6 + C_2H_4 \quad (28)$$

at high temperatures, cyclohexene dissociates to 1,3-butadiene and ethylene, which are both stable products that will not have secondary reactions in the short reaction time scales of our microreactors. Therefore, the consumption rate of cyclohexene can be calculated by,

$$\frac{dm_{cyclohexene}}{dt} = k(T,P)m_{cyclohexene} \quad (29)$$

where t is residence time and k is the pyrolysis reaction rate that is dependent on both temperature and pressure. There two methods to determine cyclohexene reaction rates. One is to use the experimentally determined reaction rate of cyclohexene by Kiefer and Shah's (Ref. [43]). Their experimental determination for the temperature-dependent cyclohexene decomposition reaction rates under different pressure conditions are

[56] Tsang, Wing, and Claudette M. Rosado-Reyes. "Unimolecular rate expression for cyclohexene decomposition and its use in chemical thermometry under shock tube conditions." *The Journal of Physical Chemistry A* 119.28 (2015): 7155-7162.

$$\log k(s^{-1}) = 102.26 - 25.3 \log T - 50.2/RT \quad (30)$$

for the low-pressure limit (0.1~0.2 atm), and

$$\log k(s^{-1}) = 96.37 - 23.6 \log T - 48.3/RT \quad (31)$$

for the high-pressure limit (0.5~0.7 atm), where R is gas constant in units of kcal / (mol K).

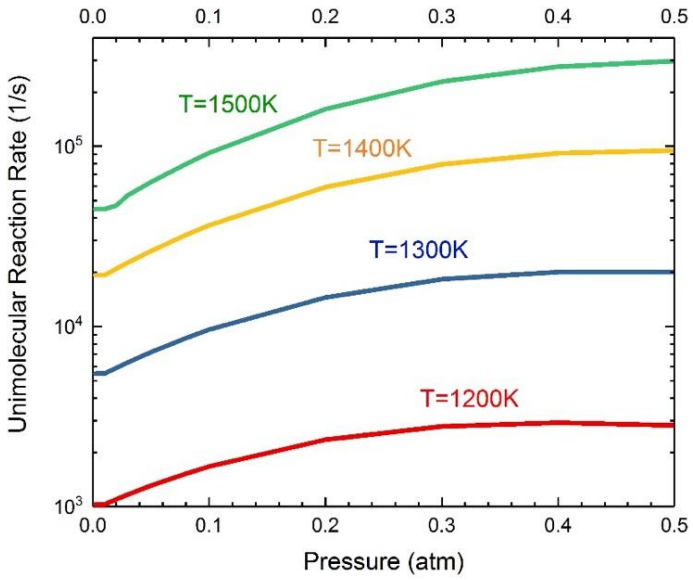

Figure 28: Cyclohexene decomposition reaction rates obtained by RRKM theory in a range of 1200 K < T < 1500 K, and 0 < P < 0.5 atm.

A more accurate pressure-dependent reaction rate for cyclohexene can be obtained by RRKM theory[57], which is shown in Figure 28. The reaction rate

[57] Gold, V., et al. "IUPAC compendium of chemical terminology." *Blackwell Science,*

is highly-dependent on temperature and will also increase when the pressure changes from 0 to 0.5 atm. Therefore, we apply RRKM theory to estimate mole fraction change, combing the data of temperature, velocity, residence time, and pressure distribution for the reactors by CFD simulation.

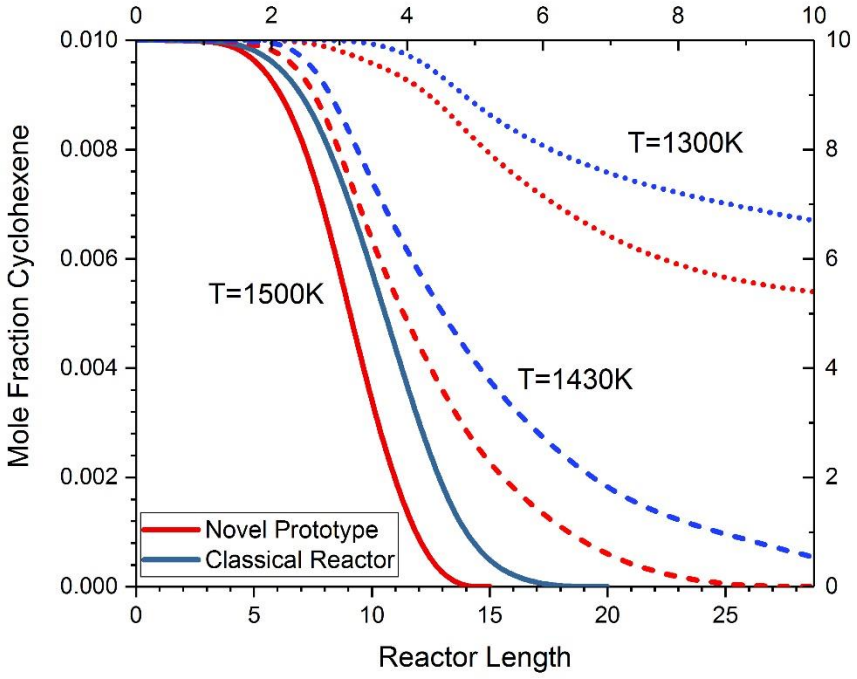

Figure 29: Center line cyclohexene mole fraction distribution as a function of the reactor length in novel prototype and classical reactor under different wall temperature (T =1300 K, 1430 K and 1500 K)

As shown in Fig. 29 and Fig. 30, the cyclohexene consumption rate in the novel prototype, to some extent, is faster than the one in the classical reactor, under various wall temperature and mass flow rate conditions. This is most likely because the novel prototype chokes the reaction flow at outlet therefore it experiences longer residence time in the reactor, even though

Oxford (1997).

the reactor's structure hardly impacts the temperature distribution.

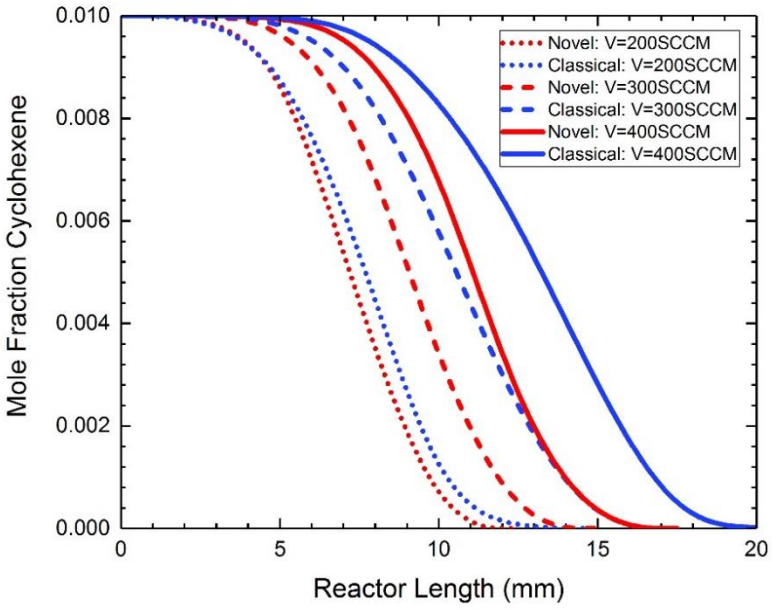

Figure 30: Center line cyclohexene mole fraction distribution as a function of the reactor length in novel prototype and classical reactor under different mass flow rate (V = 200, 300 and 400 SCCM)

It is important to mention that Fig. 29 and Fig. 30 only provides the mole fraction changing with axial position along the center line, meaning the trend in other regions of the reactor may be different. Although we do not present this data here, a reasonable prediction is provided. Reaction flow in near-wall regions will reach wall temperature earlier and be detained for longer time due to viscous effects, thus reactions in near-wall regions will happen more rapidly than those on the center line.

According to the results, when the wall temperature is 1500 K, both

cyclohexene reactants in the novel prototype and the classical reactor are exhausted before the reaction flow goes out, which means we may not observe cyclohexene (m/z: 82.1) in mass spectra under this case. At around 1430 K, the simulation results suggest that we may observe cyclohexene in the mass spectra for the classical reactor experiments but will not observe signal for cyclohexene when using the novel reactor prototype. This therefore is the ideal condition at which to demonstrate the differences in the two reactors' performances. We could also discover a difference in the reactants/products ratio for the novel and classical reactors at temperatures of 1300 K or lower since our PIMS system has the ability to determine the components of a gas mixture.

As elaborated in Chapter 2, since the PIMS signal for a dilute gas can be understood by Beer's law[58] and its strength represents the number of gas molecules detected, researchers can use the following equation to estimate the number density of gas species, n_i.

$$n_i = \frac{{S_i}^+}{CD_i\varphi(E)\sigma_i(E)} \tag{32}$$

where ${S_i}^+$ is the signal intensity, C is the constant representing all the geometry dependent factors, D_i is the mass discrimination factor, $\varphi(E)$ is

[58] Noyes, W. Albert, and Philip Albert Leighton. "Photochemistry of gases." (1966).

the photon flux, and $\sigma_i(E)$ is the energy-dependent molecular photoionization cross section. For a more straightforward method, when the 10.45 eV single photons are used to ionize all species, the ratio of cyclohexene to 1,3-butadiene and cyclohexene to ethylene can be calculated by,

$$\frac{[C_6H_{10}]}{[C_4H_6]} = \frac{S_{82}^+}{S_{54}^+}\left[\frac{D_{C_6H_{10}}\varphi_{C_6H_{10}}\sigma_{C_6H_{10}}}{D_{C_4H_6}\varphi_{C_4H_6}\sigma_{C_4H_6}}\right] \tag{33}$$

$$\frac{[C_6H_{10}]}{[C_2H_4]} = \frac{S_{82}^+}{S_{28}^+}\left[\frac{D_{C_6H_{10}}\varphi_{C_6H_{10}}\sigma_{C_6H_{10}}}{D_{C_2H_4}\varphi_{C_2H_4}\sigma_{C_2H_4}}\right] \tag{34}$$

The above experiments need to be implemented under continuous flow (CW) conditions to obtain reliable data, since the thermodynamics parameters suffer drastic changes during the pulsed flow, which would have a significant influence on the reaction rates, eventually impacting the reactants/products ratio. We are currently in the process of testing and obtaining data for the experimental system upgrade and maintenance, so the results are unavailable. However, it is believed that it will be completed in the near future. Several proposed experimental data, in sequence, including propionaldehyde decomposition and cyclohexene pyrolysis in both the classical reactor and novel prototype will be obtained in helium atmosphere under continuous flow (CW) mode.

CHAPTER 5

CONCLUSIONS

This research provides a comprehensive design of a novel microreactor for short residence time combustion, which includes structure numerical design, an alternative materials investigation, and experimental validation methods and procedures.

In the structure numerical design work, the influence of adding a nozzle structure to the existing University of Colorado Boulder microreactor system was explored using CFD calculations. The effect of adjusting the length of the existing reactor was unsurprisingly shown to influence the overall microreactor residence time. Adding a converging nozzle with exit diameter, d, was demonstrated to choke the flow within the microreactor, causing the pressure profile to no longer drop continuously through the microreactor body, but rather plateau to a stable pressure for much of the reactor. Furthermore, the nozzle exit diameter, d, was shown to be the other key design parameter in the new system, directly affecting the centerline pressure and velocity profiles within the microreactor body, as well as residence time. The length of the nozzle, G1, was found to have negligible effects. With a thorough understanding of the influence of the geometric parameters of the new microreactor structure on the thermodynamic

properties of the flow within the reactor, a new microreactor prototype with geometry (L = 28 mm, G1 = 0.75 mm, d = 0.50 mm) has been fabricated for testing. Also, continuous flow (CW) mode was demonstrated to have advantages over the current pulsed flow mode in the experiments, and upgrading the pumping to allow for CW conditions is advised before conducting next step testing since the thermodynamics environment in pulsed flow mode experiences considerable fluctuations. Additionally, the influence of uncertainty in the helium thermodynamics parameters on reactor environment predictions was modeled.

New reactor materials were investigated for future oxidation experimental capabilities. Materials were listed with pertinent attributes such as thermal conductivity, melting point, reactivity, etc. Of the most promising materials identified, we note that some oxide ceramics such as alumina ceramics and ZrO_2 may be appropriate for oxidation experiments, but need further research before final recommendation. We also consider possible micro-coating technology such as sputter coating to manufacture hybrid materials with a non-reactive inner surface should an appropriate single material not be identified.

In experimental validation part, we designed and partly implemented validation experiments with propionaldehyde and cyclohexene. In the

propionaldehyde testing, we may observe different products between the classical reactor and the prototype, since there is evidence of secondary reactions during propionaldehyde pyrolysis. These secondary reactions would be enhanced at higher pressures, thus the prototype, in which we expect to have higher pressures throughout the reactor length, may have small product distribution differences from the original reactor. For the cyclohexene experiments, we calculated the change of cyclohexene mole fraction with respect to reactor length at different temperatures and flow rates for both reactors using RRKM theory kinetics and the calculated thermodynamics profiles. A procedure for the current PIMS system to distinguish quantitative differences of products/reactants ratio between classical reactor and novel prototype is described. We expect to see that the theoretical prediction agrees well with experimental results in oncoming experiments.

The work in this thesis offers insight on the relationship between microreactor geometry, internal flow dynamics, and chemical kinetics. From this work, we expect advancements in microreactor design, which will help researchers have a better understanding on short residence time combustion processes and achieve more precise and reliable analytical chemical results.

REFERENCES

[1] "Electric Power Monthly with Data for July 2017." *U.S. Energy Information Administration*

[2] Brown, James S., et al. "Thoracic and respirable particle definitions for human health risk assessment." *Particle and fibre toxicology* 10.1 (2013): 12.

[3] Chen, Peter, et al. "Flash pyrolytic production of rotationally cold free radicals in a supersonic jet. Resonant multiphoton spectrum of the 3p2A2". rarw. X2A2" origin band of methyl." *The Journal of Physical Chemistry* 90.11 (1986): 2319-2321.

[4] Buckingham, Grant T., et al. "The thermal decomposition of the benzyl radical in a heated micro-reactor. I. Experimental findings." *The Journal of chemical physics* 142.4 (2015): 044307.

[5] Buckingham, Grant T., et al. "The thermal decomposition of the benzyl radical in a heated micro-reactor. II. Pyrolysis of the tropyl radical." *The Journal of chemical physics* 145.1 (2016): 014305.

[6] Urness, Kimberly N., et al. "Pyrolysis Pathways of the Furanic Ether 2-Methoxyfuran." *The Journal of Physical Chemistry A*119.39 (2015): 9962-9977.

[7] Porterfield, Jessica P., et al. "Isomerization and fragmentation of cyclohexanone in a heated micro-reactor." *The Journal of Physical Chemistry A* 119.51 (2015): 12635-12647.

[8] Porterfield, Jessica P., et al. "Pyrolysis of the Simplest Carbohydrate, Glycolaldehyde (CHO− CH2OH), and Glyoxal in a Heated Microreactor." *The Journal of Physical Chemistry A* 120.14 (2016): 2161-2172.

[9] Porterfield, Jessica P., et al. "Thermal Decomposition of Potential Ester Biofuels Part I: Methyl Acetate and Methyl Butanoate." *The Journal of Physical Chemistry A* (2017).

[10] Haswell, Stephen J., et al. "The application of micro reactors to synthetic chemistry." *Chemical Communications* 5 (2001): 391-398.

[11] Roberge, Dominique M., et al. "Microreactor technology: a revolution for the fine chemical and pharmaceutical industries?" *Chemical engineering & technology* 28.3 (2005): 318-323.

[12] Chen, Peter, et al. "Flash pyrolytic production of rotationally cold free radicals in a supersonic jet. Resonant multiphoton spectrum of the 3p2A2". rarw. X2A2" origin band of methyl." *The Journal of Physical Chemistry* 90.11 (1986): 2319-2321.

[13] Blush, Joel A., et al. "Photoionization mass and photoelectron spectroscopy of radicals, carbenes, and biradicals." *Accounts of chemical research* 25.9 (1992): 385-392.

[14] Lockyer, Nicholas P., and John C. Vickerman. "Single photon ionisation mass spectrometry using laser-generated vacuum ultraviolet photons." *Laser Chemistry* 17.3 (1997): 139-159.

[15] Van Bramer, S. E., and M. V. Johnston. "Tunable, coherent vacuum ultraviolet radiation for photoionization mass spectrometry." *Applied spectroscopy* 46.2 (1992): 255-261.

[16] Steenvoorden, R. J. J. M., et al. "Laser single photon ionization mass spectrometry of linear, branched and cyclic hexanes." *International Journal of Mass Spectrometry and Ion Processes*107.3 (1991): 475-489.

[17] Mamyrin, B. A., et al. "The massreflect ron, a new non-magnetic time-of-flight mass spectrometer with high resolution." *Zh. Eksp. Teor. Fiz* 64 (1973): 82-89.

[18] Mamyrin, B. A. "Time-of-flight mass spectrometry (concepts, achievements, and prospects)." *International Journal of Mass Spectrometry* 206.3 (2001): 251-266.

[19] Susi, Heino, and D. Michael Byler. "[13] Resolution-enhanced fourier transform infrared spectroscopy of enzymes." *Methods in enzymology* 130 (1986): 290-311.

[20] Christy, Alfred A., Yukihiro Ozaki, and Vasilis G. Gregoriou. *Modern Fourier transform infrared spectroscopy*. Elsevier, 2001.

[21] Zhang, Xu, et al. "Intense, hyperthermal source of organic radicals for matrix-isolation spectroscopy." *Review of scientific instruments* 74.6 (2003): 3077-3086.

[22] Vasiliou, AnGayle, et al. "Thermal decomposition of furan generates propargyl radicals." *The Journal of Physical Chemistry A* 113.30 (2009): 8540-8547.

[23] Vasiliou, AnGayle K., et al. "Thermal decomposition of CH3CHO studied by matrix infrared spectroscopy and photoionization mass spectroscopy." *The Journal of chemical physics* 137.16 (2012): 164308.

[24] Laidler, K. J., and M. T. H. Liu. "The mechanism of the acetaldehyde pyrolysis." *Proceedings of the Royal Society of London A: Mathematical, Physical and Engineering Sciences*. Vol. 297. No. 1450. The Royal Society, 1967.

[25] Urness, Kimberly N., et al. "Pyrolysis of furan in a microreactor." *The Journal of chemical physics* 139.12 (2013): 124305.

[26] Urness, Kimberly N., et al. "Pyrolysis Pathways of the Furanic Ether 2-Methoxyfuran." *The Journal of Physical Chemistry A*119.39 (2015): 9962-9977.

[27] Jarvis, Mark W., et al. "Direct detection of products from the pyrolysis of 2-phenethyl phenyl ether." *The Journal of Physical Chemistry A* 115.4 (2011): 428-438.

[28] Zhang, Taichang, et al. "Pyrolysis of methyl tert-butyl ether (MTBE). 1. Experimental study with molecular-beam mass spectrometry and tunable synchrotron VUV photoionization." *The Journal of Physical Chemistry A* 112.42 (2008): 10487-10494.

[29] Guan, Qi, et al. "The properties of a micro-reactor for the study of the unimolecular decomposition of large molecules." *International Reviews in Physical Chemistry* 33.4 (2014): 447-487.

[30] Holman, Jack P. Heat transfer. Vol. 2. New York: McGraw-hill, 1986.

[31] Cengel, Yunus A., and Michael A. Boles. "Thermodynamics: an engineering approach." Sea 1000 (2002): 8862.

[32] Moukalled, F., L. Mangani, and M. Darwish. "The finite volume method in computational

fluid dynamics." (2016).

[33] Petersen, Helge. The properties of helium: density, specific heats, viscosity, and thermal conductivity at pressures from 1 to 100 bars and from room temperature to about 1800 K. 1970.

[34] Fluent, A. N. S. Y. S. "Ansys fluent theory guide." ANSYS Inc., USA 15317 (2011): 724-746.

[35] ANSYS, ICEM CFD. "13: geometry and mesh generation preprocessor." Ansys Inc (2012).

[36] Ambatipudi, Vaidehi. "SIMPLE Solver for Driven Cavity Flow Problem." Department of Mechanical Engineering, Purdue University (2010).

[37] Mangani, L., and C. Bianchini. "Heat transfer applications in turbomachinery." Proceedings of the OpenFOAM International Conference. 2007.

[38] Tannehill, John C., Dale A. Anderson, and Richard H. Pletcher. "Computational fluid mechanics and heat transfer, Series in computational and physical processes in mechanics and thermal sciences." (1997).

[39] Warner, Brian J., et al. "Products from Pyrolysis of Gas-Phase Propionaldehyde." The Journal of Physical Chemistry A 119.1 (2014): 14-23.

[40] Tranter, R. S., et al. "Calibration of reaction temperatures in a very high-pressure shock tube using chemical thermometers." International Journal of Chemical Kinetics 33.11 (2001): 722-731.

[41] Heyne, Joshua S., and Frederick L. Dryer. "Uncertainty analysis in the use of chemical thermometry: A case study with cyclohexene." The Journal of Physical Chemistry A 117.26 (2013): 5401-5406.

[42] Kiefer, John H., and Jatin N. Shah. "Unimolecular dissociation of cyclohexene at extremely high temperatures: behavior of the energy-transfer collision efficiency." J. Phys. Chem.;(United States) 91.11 (1987).

[43] Bird, Graeme Austin. "Molecular gas dynamics." *NASA STI/Recon Technical Report A* 76 (1976).

[44] Munro, R. G., and S. J. Dapkunas. "Corrosion characteristics of silicon carbide and silicon nitride." *Journal of research of the National Institute of Standards and Technology* 98.5 (1993): 607.

[45] Auerkari, Pertti. *Mechanical and physical properties of engineering alumina ceramics*. Espoo: Technical Research Centre of Finland, 1996.

[46] Shand, Mark A. *The chemistry and technology of magnesia*. John Wiley & Sons, 2006.

[47] Nielsen, Ralph. "Zirconium and zirconium compounds." *Ullmann's Encyclopedia of Industrial Chemistry* (2000).

[48] Rose, Lars. *On the degradation of porous stainless steel in low and intermediate temperature solid oxide fuel cell support materials*. Diss. University of British Columbia,

2011.

[49] "Titanium". *Columbia Encyclopedia (6th ed.). New York:* Columbia University Press. *2000–2006.* ISBN 0-7876-5015-3. *Archived from the original on 18 November 2011.*

[50] Walsh, Patrick N., Jean M. Quets, and Robert A. Graff. "Kinetics of the Oxygen—Tungsten Reaction at High Temperatures." *The Journal of Chemical Physics* 46.3 (1967): 1144-1153.

[51] Kelly, P.F. (2015). *Properties of Materials*. CRC Press. p. 355. ISBN 978-1-4822-0624-1.

[52] Weast, Robert (1984). *CRC, Handbook of Chemistry and Physics*. Boca Raton, Florida: Chemical Rubber Company Publishing. pp. E110. ISBN 0-8493-0464-4.

[53] Parish, R. V. "Organogold chemistry: II reactions." *Gold Bulletin*30.2 (1997): 55-62.

[54] Nickel, *Palladium and Platinum (Comprehensive Organometallic Chemistry II)* R.J. Puddephatt (Editor) 2002 0080423167

[55] Tsang, Wing, and Claudette M. Rosado-Reyes. "Unimolecular rate expression for cyclohexene decomposition and its use in chemical thermometry under shock tube conditions." *The Journal of Physical Chemistry A* 119.28 (2015): 7155-7162.

[56] Echlin, P. "Sputter coating techniques for scanning electron microscopy." *Scanning Electron Microsc* 2 (1975): 217-224.

[57] Gold, V., et al. "IUPAC compendium of chemical terminology." *Blackwell Science, Oxford* (1997).

[58] Noyes, W. Albert, and Philip Albert Leighton. "Photochemistry of gases." (1966).

APPENDIX

Here, we describe detailed calculation procedures and settings for the microreactor numerical design using the simulation software, ANSYS Fluent, which is a commercial CFD software package used for simulating complex fluid flows in a large range of applicable cases from uncompressible to highly-compressible flow. However, since ANSYS Fluent is not an open-source software, there are no source codes that we can provide. Instead, significant numerical methods settings and control equations are listed here such that researchers can repeat our study.

1. Tetrahedral mesh made by ICEM:

Structured tetrahedral mesh is a general mesh style for three-dimensional model discretization. It is suitable for a large number of model profiles, is easy to build, and has a low probability of error with respect to structural geometry.

2. Density-based solver:

The density-based solver couples equation groups that can solve the continuity, momentum, energy, and species transport equations

simultaneously. For high-speed compressible flow, the density-based solver typically requires a lower number of iterations for convergence in comparison to pressure-based solvers.

3. SIMPLE algorithm

The SIMPLE scheme is a numerical procedure widely applied to solve Navier-Stokes equations for uncompressible flow. It fundamentally supposes that the velocity field and assumed pressure field operate independently, and that the correction to the pressure field is obtained from solutions of the mass conversation equation for the velocity field. The revised algorithm allows the initial velocity and pressure fields to be assumed independently to extend the application of the SIMPLE method to compressible flow.

4. Second-order-upwind scheme

The second-order-upwind scheme is a numerical discretization method to solve partial differential equations, which can obtain more accurate and stable solutions than traditional single-order upwind schemes.

5. Control equations and Helium properties

5.1 Steady state continuity equation for compressible flow:

$$\nabla \cdot \left(\rho \vec{U}\right) = 0$$

5.2 Steady state conservation of momentum equation for compressible flow:

$$\rho\left(\vec{U} \cdot \nabla\right)\vec{U} = \vec{f} - \nabla p + \mu\nabla^2\vec{U} - \frac{2}{3}\mu\nabla\left(\nabla \cdot \vec{U}\right)$$

5.3 Steady state conservation of energy equation for compressible ideal gas flow:

$$c_p\nabla \cdot \left(\rho\vec{U}T\right) = \nabla \cdot (k\nabla T) + \lambda\Psi + \mu\Phi + \dot{Q}$$

where

$$\Psi = \left(\frac{\partial u}{\partial x} + \frac{\partial v}{\partial y} + \frac{\partial w}{\partial z}\right)^2$$

$$\Phi = 2\left[\left(\frac{\partial u}{\partial x}\right)^2 + \left(\frac{\partial v}{\partial y}\right)^2 + \left(\frac{\partial w}{\partial z}\right)^2\right] + \left(\frac{\partial u}{\partial y} + \frac{\partial v}{\partial x}\right)^2 + \left(\frac{\partial v}{\partial z} + \frac{\partial w}{\partial y}\right)^2 + \left(\frac{\partial w}{\partial x} + \frac{\partial u}{\partial z}\right)^2$$

5.4 Helium thermal conductivity and dynamics viscosity experimental formulas:

$$k = 2.682 \cdot 10^{-3}(1 + 1.123 \cdot 10^{-3}P)T^{\left(0.71(1-2\cdot 10^{-4}P)\right)}\ [W/(m * K)]$$

$$\mu = 3.67\times 10^{-7} \cdot T^{0.7}\ [Pa.s]$$

where T and P have units of Kelvin and Bar respectively.